

AD-A121 298

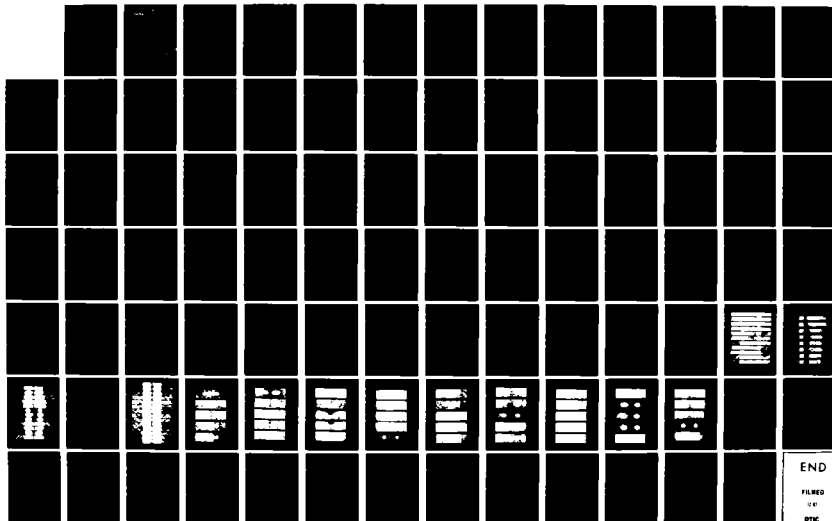
COMPOSITE DEFECT SIGNIFICANCE(U) MATERIALS SCIENCES
CORP SPRING HOUSE PA S N CHATTERJEE ET AL. 13 JUL 82
MSC/TFR/1208/1107 NADC-80048-60 N62269-80-C-0271

1/1

UNCLASSIFIED

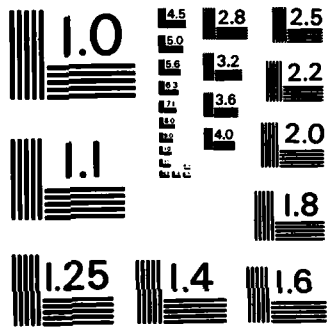
F/G 11/4

NL



END

FILMED
10
DTIC



MICROCOPY RESOLUTION TEST CHART
NATIONAL BUREAU OF STANDARDS-1963-A



12

AD A121290



Materials Sciences Corporation

COMPOSITE DEFECT SIGNIFICANCE

S. N. CHATTERJEE AND R. B. PIPES

13 JULY 1982

Approved for Public Release; Distribution Unlimited



Prepared for:
NAVAL AIR DEVELOPMENT CENTER
Warminster, PA

82 11 05 053

DTIC FULL COPY

NOTICES

REPORT NUMBERING SYSTEM - The numbering of technical project reports issued by the Naval Air Development Center is arranged for specific identification purposes. Each number consists of the Center acronym, the calendar year in which the number was assigned, the sequence number of the report within the specific calendar year, and the official 2-digit correspondence code of the Command Office or the Functional Directorate responsible for the report. For example: Report No. NADC-78015-20 indicates the fifteenth Center report for the year 1978, and prepared by the Systems Directorate. The numerical codes are as follows:

CODE	OFFICE OR DIRECTORATE
00	Commander, Naval Air Development Center
01	Technical Director, Naval Air Development Center
02	Comptroller
10	Directorate Command Projects
20	Systems Directorate
30	Sensors & Avionics Technology Directorate
40	Communication & Navigation Technology Directorate
50	Software Computer Directorate
60	Aircraft & Crew Systems Technology Directorate
70	Planning Assessment Resources
80	Engineering Support Group

PRODUCT ENDORSEMENT - The discussion or instructions concerning commercial products herein do not constitute an endorsement by the Government nor do they convey or imply the license or right to use such products.

APPROVED BY:



DATE:

7/13/82

Unclassified

SECURITY CLASSIFICATION OF THIS PAGE (When Data Entered)

REPORT DOCUMENTATION PAGE		READ INSTRUCTIONS BEFORE COMPLETING FORM
1. REPORT NUMBER NADC-80048-60	2. GOVT ACCESSION NO. AD-A121290	3. RECIPIENT'S CATALOG NUMBER
4. TITLE (and Subtitle) COMPOSITE DEFECT SIGNIFICANCE		5. TYPE OF REPORT & PERIOD COVERED Final Report 9/30/80 - 8/31/81
		6. PERFORMING ORG. REPORT NUMBER MSC TFR 1208/1107
7. AUTHOR(s) S. N. Chatterjee R. B. Pipes		8. CONTRACT OR GRANT NUMBER(s) N62269-80-C-0271
9. PERFORMING ORGANIZATION NAME AND ADDRESS Materials Sciences Corporation Gwynedd Plaza II, Bethlehem Pike Spring House, PA 19477		10. PROGRAM ELEMENT, PROJECT, TASK AREA & WORK UNIT NUMBERS
11. CONTROLLING OFFICE NAME AND ADDRESS Naval Air Development Center (Code 6063) Warminster, PA 18974		12. REPORT DATE 13 July 1982
		13. NUMBER OF PAGES 96
14. MONITORING AGENCY NAME & ADDRESS (if different from Controlling Office)		15. SECURITY CLASS. (of this report) Unclassified
		15a. DECLASSIFICATION/DOWNGRADING SCHEDULE
16. DISTRIBUTION STATEMENT (of this Report) Approved for public release, distribution unlimited.		
17. DISTRIBUTION STATEMENT (of the abstract entered in Block 20, if different from Report)		
18. SUPPLEMENTARY NOTES		
19. KEY WORDS (Continue on reverse side if necessary and identify by block number) Composite Materials, Non-destructive Testing, Non-destructive Evaluation, Defect Characterization, Graphite/Epoxy, Fracture Mechanics Delamination Defect Criticality, Fatigue		
20. ABSTRACT (Continue on reverse side if necessary and identify by block number) State of the art of defect criticality assessment in structural composite laminates has been summarized and significance of other ongoing programs has been reviewed through literature survey and organization of a limited attendance symposium on the subject. A number of tests have been performed to determine the range of validity of criticality criteria for disbonds in laminated beam and plate type structures, which were developed in previous related programs. Data correlation studies have shown the usefulness		

DD FORM 1473, EDITION OF 1 NOV 65 IS OBSOLETE

Unclassified

-i- SECURITY CLASSIFICATION OF THIS PAGE (When Data Entered)

cont'd

Unclassified

SECURITY CLASSIFICATION OF THIS PAGE(When Data Entered)

20. of linear elastic fracture mechanics approach, methods of stress analysis based on 2-D elasticity and modified laminated plate theories as well as semi-empirical growth laws for cyclic loading for assessing growth of disbonds under transverse shear.

Accession For	
NTIS GRA&I	<input checked="" type="checkbox"/>
DTIC TAB	<input type="checkbox"/>
Unannounced	<input type="checkbox"/>
Justification	
By	
Distribution/	
Availability Codes	
Dist	Avail and/or Special
A	

DTIC
COPY
INSPECTION
2

SUMMARY

The state of the art for assessment of defect criticality in structural composite laminates has been reviewed and summarized. The significance of related ongoing programs has been reviewed through a literature survey and the organization of a limited attendance symposium on the subject.

Tests have been performed to determine the range of validity of criticality criteria for disbonds in laminated beam and plate type structures, which were developed in previous related programs. Data correlation studies have shown the usefulness of a linear elastic fracture mechanics approach, of methods of stress analysis based on 2-D elasticity and modified laminated plate theories, as well as of semi-empirical growth laws for cyclic loading, for assessing growth of disbonds under transverse shear.

FOREWORD

This report summarizes the work done for the Naval Air Development Center, Warminster, PA 18974, under contract N 62269-80-C-0271 during the period September 30, 1980 to August 5, 1981.

The authors wish to express their sincere appreciation to Dr. B. Walter Rosen and Dr. W. R. Scott for various suggestions and discussions during different stages of this work. Sincere thanks are due to Mr. Robert A. Blake, Jr. for his extensive work in the experimental studies.

The proceedings of the Symposium on "Nondestructive and Analytical Evaluation of Criticality of Defects in Structural Composite Laminates," which was sponsored under the contract and was held in Philadelphia on November 24-25, 1980, is a part of the final report documentation. These proceedings are contained in MSC TPR 1107/1158.

Approved:



B. Walter Rosen
Program Director

TABLE OF CONTENTS

	<u>Page</u>
INTRODUCTION.	1
BACKGROUND.	3
LITERATURE SEARCH	5
SYMPOSIUM ON DEFECT CRITICALITY	7
DISCUSSION ON STATE OF THE ART.	12
EXPERIMENTAL PROGRAM.	15
TASK I. - EFFECTS OF DISBOND LOCATION	15
Test Method	15
Fabrication and Sample Geometry	16
Data.	17
TASK II. - EFFECTS OF SHARPNESS OF DISBOND TIPS	17
Test Method	17
Fabrication and Sample Geometry	17
Data.	18
TASK III. - GROWTH OF CIRCULAR DISBONDS UNDER CYCLIC LOADING	18
Test Method	18
Data.	20
DATA CORRELATION STUDIES.	21
TASK I. - EFFECT OF DISBOND LOCATION.	21
TASK II. - EFFECT OF SHARPNESS OF DISBOND TIPS.	25
TASK III. - PROPAGATION OF DISBOND IN FATIGUE	26
DISCUSSIONS AND CONCLUSIONS	30
REFERENCES.	32
BIBLIOGRAPHY B1 - NOTCHED LAMINATES	33
BIBLIOGRAPHY B2 - DELAMINATIONS	35
TABLES.	39
FIGURES	56

LIST OF TABLES

<u>Table</u>		<u>Page</u>
1	Laminate Type and Defect Location - Task I	39
2	Test Data for Type A Laminates - Task I	40
3	Test Data for Type B Laminates - Task I	41
4	Test Data for Type C Laminates - Task I	42
5	Load Drop Data for Type A Laminates - Task I.	43
6	Test Data for Blunt (B) and Sharp (S) Delaminations - Task II	44
7	Details of Samples with Circular Disbonds Tested in Fatigue - Task III	45
8	Data Correlation for Type A Laminates - Task I.	47
9	Data Correlation for Type B Laminates - Task I.	49
10	Data Correlation for Type C Laminates - Task I.	51
11	Calculated Values of Critical Energy Release Rates for Blunt and Sharp Tips.	53
12	Elastic Properties of 0° Layer and Stiffness of (0 ₄ /±45 ₂ /∓45 ₂ /0 ₄) _s Laminate	54
13	Stiffnesses of (0 ₄ /±45 ₂ /∓45 ₂ /0 ₄) and (0 ₄ /±45 ₂ /∓45 ₂ /0 ₄) ₃ Laminates	55

LIST OF FIGURES

<u>Figure</u>		<u>Page</u>
1	Test Geometry for Three Point Bend Tests.	56
2	Representative C-scans Prior to Loading	57
3	Representative C-scans After Load Drop and Prior to Complete Failure-Type A Laminates.	58
4	C-scans of Sharp Crack Specimens - Task II.	59
5	Blunt Crack Sample Geometry	60
6	C-scans of Blunt Crack Specimens - Task II.	61
7	Flaw Growth in Sample 3-1RO-1, S = 0.5.	62
8	Flaw Growth in Sample 3-125RO-1, S = 0.5.	63
9	Flaw Growth in Sample 3-150RO-1, S = 0.5.	64
10	Flaw Growth in Sample 3-1R+25-2, S = 0.5.	65
11	Flaw Growth in Sample 3-1R-25-2, S = 0.5.	66
12	Flaw Growth in Sample 3-125R+25-1, S = 0.75	67
13	Flaw Growth in Sample 3-125R-25-2, S = 0.5.	68
14	Flaw Growth in Sample 3-150R+25-3, S = 0.75	69
15	Flaw Growth in Sample 3-150R-25-1, S = 0.5.	70
16	Measurement Locations for Four Crack Fronts	71
17	Failure Loads for Disbonds of 2.54 cm. Length in 2.54 cm. Wide Beams - Type A Laminates	72
18	Failure Loads for Disbonds of 2.54 cm. Length in 2.54 cm. Wide Beams - Type B Laminates	73
19	Failure Loads for Disbonds of 2.54 cm. Length in 2.54 cm. Wide Beams - Type C Laminates	74
20	Variation of G_{II} with Dimensions for Flaws at Z = ±0.25H.	75
21	Variation of G_{III} with Dimensions for Flaws at Z = ±0.25H.	76

LIST OF FIGURES (Cont'd)

<u>Figure</u>		<u>Page</u>
22	Variation of G_I with Dimensions of Flaw at $Z = \pm 0.25H$	77
23	Variation of G_I and G_{II} with L_1/L_2	78
24	L_1 vs. N , Sample 3-1RO-1, $S = 0.5$	79
25	L_1 vs. N , Sample 3-1R-25-2, $S = 0.5$	80
26	L_1 vs. N , Sample 3-125RO-2, $S = 0.5$	81
27	L_1 vs. N , Sample 3-150R+25-3, $S = 0.75$	82
28	L_1 vs. N , Sample 3-150R-25-1, $S = 0.5$	83
29	Growth of Disbonds in Midplane, $Z = 0$	84
30	Growth of Disbonds at $Z = \pm 0.25H$	85

INTRODUCTION

Nondestructive evaluation of criticality of defects in a composite structure or a structural component poses a challenging problem to the analyst. The first step for such an evaluation is determination of the size, shape and location of an isolated defect or of a number of closely spaced defects by nondestructive inspection techniques. The next step is to assess residual stiffness, strength or life in the presence of these defects by the use of appropriate analytical methods for stress analysis, as well as to predict failure and the expected growth mechanism of the defects. At the present time only limited use is made of NDE concepts for quantitative evaluation of residual properties because of the limitations of contemporary inspection techniques and analytical methods of assessing flaw criticality.

Work under three previous contracts, N62269-77-0092, N62269-78-C-0111 and N62269-79-C-0209, were directed towards the development of a NDE methodology for assessing criticality of isolated disbonds in one- and two-dimensional laminated structural members under transverse shear and/or compressive loads. These investigations consisted of analytical modeling, as well as nondestructive and destructive tests to establish criticality criteria as functions of stress level, fatigue cycles and environment. Mechanisms of growth of flaws, and failure predicted by analytical methodology, were correlated with experimental data with reasonable accuracy. Further tests were, however, deemed necessary to establish the range of validity of the proposed methodology.

Subsequent to the start of work under the three investigations discussed above, other programs were initiated in the general area of defect significance in composite materials. It appeared worthwhile to review the approaches taken in such programs for assessment of flaw criticality. Therefore, the objectives of the current work were:

1. To summarize and assess significant on-going programs in the area of flaw criticality in composites so as to obtain an integrated picture of the current state of the art in this field.
2. To conduct a number of critical tests and data correlation studies, to establish the range of validity of the criticality criteria developed during the previous investigations as applied to disbonds with 1-D and 2-D planforms.

BACKGROUND

In order to arrive at a definition of a critical flaw, it is necessary to formulate an analytical model which is capable of predicting the direction and rate of its growth and its critical size (at failure). Due to the complexity of the problem of failure in composite laminates, it is impossible for a single analytical model to encompass the whole spectrum of fracture and fatigue behavior. In other words, different analytical models should be developed to predict growth of different types of flaws such as surface flaws, through-the-thickness notches and delaminations.

An initial investigation of flaw criticality (ref. 1) was concerned with slit notches and interlaminar disbonds in short beams under static and fatigue loads. The analysis employed for interlaminar disbonds was of the "strength of materials" type. The values of the specific adhesive surface fracture energy, as determined from correlation of test data for quasi-static growth of disbonds with analytical calculations, showed some discrepancy. For this reason, a more sophisticated two-dimensional stress analysis for prediction of quasi-static disbond propagation was later developed (ref. 2). It was observed that the simple "strength of materials" solution yields estimates of failure load close to those obtained by the use of 2-D elasticity theory for sufficiently large values of the ratio of disbond length to laminate thickness. The simple solution, however, becomes increasingly nonconservative as the disbond length is reduced. In the latter study, the stress intensity factors calculated from the 2-D elasticity solution were used to demonstrate the usefulness of the commonly used semiempirical crack growth law for predicting growth of disbonds under cyclic shear. Test data from a series of tests and curve fitting procedures were employed to obtain the two constants used in the crack growth law. A criterion for criticality of disbonds in a

laminate under compressive loads was also developed and tested with the help of experimental data. This criterion predicts a buckling type of failure of unsupported parts of the compression skin.

The criticality of disbonds with circular and nearly elliptic planforms in laminated plates under transverse shear and compressive loads were considered in reference 3. As in the case of 1-D disbonds, the failure under compressive loads was found to be due to buckling of the unsupported skin. Growth of disbonds under cyclic shear was found to occur in a slow regular pattern. An analytical methodology based on a modified laminated plate theory was developed which yields flaw criticality criteria and/or growth laws under compressive loads as well as quasi-static and cyclic shear stresses. Because of the nature of the theory being used for stress analysis, the theory is likely to yield higher values of failure load for disbonds of very small size. Further, in a majority of tests conducted, the flaws were located in the mid-plane of the laminate and between two layers of the same orientation. Therefore, more tests were conducted in the present study to examine the range of validity of the proposed criticality criteria as regards to its location, size, shape and sharpness of the disbond tips.

Several other current studies in the area of defect significance (ref. 4 for example) have some aspects in common with the investigations discussed above, although the dominant stress-states and other details in such studies are different. It is, therefore, of interest to assess the significance of results of such programs as applied to defects of the type under consideration. Such an assessment was attempted in this study through literature search and organization of a symposium on defect criticality in structural composite laminates.

LITERATURE SEARCH

A literature search on Defect Criticality in Composite Materials, covering a period of the past three years, was conducted through the U.S. Small Business Administration by the Delaware Technical and Community College. NTIS and NASA data bases were utilized in this search. In addition to this search, a study of recent relevant works was also conducted. Results are given in the attached bibliographies B1 and B2. Bibliography B1 lists the works related to criticality of through-the-thickness flaws (cracks, notches or holes) under static and cyclic loading. It is known that these kinds of flaws give rise to interlaminar damages as well as matrix or fiber-matrix interface damages parallel to the fibers in some of the laminae in a laminated composite. Therefore, a majority of these studies is focused on study and detection of such damage growths. Use of fracture mechanics methodologies and semiempirical crack growth laws as well as crack growth in unidirectional and random fiber reinforced composites are considered in other studies. Use of NDI is reported in a few studies (B1.15, 1.17 for example).

Bibliography B2 lists works related to delamination growth in composite materials. B2.1 lists the studies on delamination growth in the Mode I (peel) mechanism. Test methods, as well as applications to static and cyclic loading, are examined. Growth of delaminations in Mode II alone is considered in very few studies, as listed in B2.2. Test specimen designs for Mode II and Mode III extensions are also attempted in B2.1.7.

Combined mode effects due to the presence of surface flaws, notch or free edges, are considered in several works listed in B2.3. All of the works listed in B2.1, B2.2 and B2.3 are based on calculation of strain energy release rates and/or stress intensity factors. A majority of the studies listed in B2.3 makes use of 2-D finite element calculations and some of these utilize special 2-D crack tip elements near the delaminations. The

study B2.1.7 makes use of 3-D finite elements. Transverse cracking in 90° layers is examined in B2.3.1 and B2.3.7.

Effects of fatigue and compression loads are examined in the works listed in B2.4. Debonding between metals and composites are considered in B2.4.5, B2.4.6 and B2.4.8. Other studies show that fatigue loading induces a considerable amount of delamination growth before final failure may be expected. Under compression fatigue, final failure is expected due to buckling of disbonded skins. Calculation of buckling loads for disbonded compression skins is also reported in B2.2.1.

A considerable amount of experimental work is reported in many of the studies for determination of fracture toughness or critical strain energy release rates and growth laws under cyclic loading as well as residual strength. Use of nondestructive inspection techniques is also reported in some studies.

SYMPOSIUM ON DEFECT CRITICALITY

A limited attendance symposium on "Nondestructive and Analytical Evaluation of Criticality of Defects in Structural Composite Laminates" was organized. The meeting was held on November 24-25, 1980 in Philadelphia. Twenty-seven research workers active in the areas of materials and structures attended the symposium. Abstracts and vu-graphs of presentations, as well as the comments and discussions by the attendees, can be found in the informal Symposium Proceedings, MSC TPR 1107/1158. The symposium was arranged for the purpose of reviewing the state of the art of defect criticality assessment and providing a forum for discussion on future research needs in the disciplines of structural analysis as well as materials development. Presentations and discussions dealt with a variety of analytical and experimental tools for assessment of defect criticality. In addition, two sessions were devoted to general discussions on needs and capabilities as well as recommendations for future research.

Most of the presentations focused on ongoing research activities. Work on various types of defects were reported, and the area of greatest activity appeared to be the growth of delaminations under quasi-static and cyclic loading. Delaminations of comparatively large size as well as small inherent flaws near edges and those inside a composite were considered. Studies on dispersed voids and through-the-thickness defects were also reported. The presentations contained in the proceedings are summarized below for the purpose of assessing the state of the art, which is discussed in the next section.

1. "Delamination in Graphite/Epoxy Composites" by D. J. Wilkins. This work deals with the use of 3-D brick finite elements for calculation of strain energy release rates for delamination type defects in aircraft structural components as well as test coupons designed for measurement of critical values of Mode I

and Mode II energy release rates. Growth laws under cyclic loading are also determined experimentally. Use of such laws in predicting damage growth under fatigue loading is also considered.

2. "Flaw Criticality in Graphite/Epoxy Composites" by R. B. Pipes and "Analytical Modeling of Delaminations in Laminated Composites" by S. N. Chatterjee. These works deal with the studies conducted by Materials Sciences Corporation under two previous contracts, N62269-79-C-0209 and N62269-78-C-0111. Use of ultrasonic C-scans for monitoring damage growth is considered in the first work. In the second study, 2-D elasticity theory is used for through-the-thickness disbonds in beam-type structures and a modified laminated plate theory is utilized for elliptic disbonds in plate type structures for the purpose of strain energy release rate calculations. Experimental-analytical data correlations are performed for determining Mode II critical energy release rate and crack growth laws under cyclic loading. Quasi-static buckling loads for disbonded compression skins are also calculated and compared with experimental data.
3. "Investigation of Damage Growth in Composites" by M. M. Ratwani. This work is based on the fact that inherent disbonds usually grow under fatigue loading and it is expected that such disbonds will grow in the interface where the transverse shear stress is a maximum and exceeds a threshold value. Such shear stresses near a hole or a free edge are calculated by a finite element method on the assumption that the flaws are absent. Although the growth of the disbonds is usually two-dimensional, it is postulated that it can be characterized by a crack growth law of the self-similar type. Residual strength and/or lifetime under constant ampli-

tude loading or spectrum fatigue loading are calculated on the assumption that buckling is the mechanism of final failure. Buckling stress is computed by a formula similar to the Euler type column buckling equation with a multiplier and, therefore, the critical value of the characteristic dimension of the flaw can be computed. Some of the parameters in the model are chosen to fit experimental results from compression fatigue tests. Attempts are made to monitor damage growth by x-ray radiography and C-scans.

4. "The Criticality of Free Edge Delaminations in Graphite/Epoxy Laminates" by A. S. D. Wang. Strain energy release rates are calculated by the use of 2-D finite elements. Possibilities of delamination growth near free edges, as well as near transverse cracks in the 90° layers, are examined and the sequence of the growth of transverse cracks and delaminations is postulated for some laminate configurations.
5. "Flaw Induced Delaminations in Fatigued Graphite/Epoxy Composites: Effect on Lifetime and Ultrasonic Detection" by R. J. Richards. It is shown in this study that delamination fatigue failures in laminated composites initiate at intrinsic laminar flaws. Ultrasonic detection of flaws is correlated with optical observations. An attempt is made to find a relationship between lifetime and the stress intensity factor range, ΔK_{II} .
6. "Development of Acceptance Criteria for Graphite/Epoxy Structures" by B. L. Riley. This is a study on the effect of porosity on failure under combined action of compressive and shear stresses. Naturally and artificially induced porosities are compared and a test program is carried out to determine the failure criteria under combined stresses.

7. "Progressive Failure Strength Model for Advanced Composite Laminates" by D. Y. Konishi. Progressive lamina by lamina failure near a crack or a hole is examined. Stresses are computed by anisotropic elasticity theory. Failure in a lamina is assumed to occur when the stresses at a characteristic dimension away from the crack tip or hole boundary fall on a failure envelope. Stiffnesses of the laminate are adjusted depending on fiber or matrix failure in the failed lamina. Failure of the laminate occurs when the principal load bearing lamina fails. Analytical predictions are compared with experimental data.
8. "Nondestructive and Analytical Evaluation of Criticality of Defects in Structural Laminates - An Airframe Contractor's Perspective" by J. A. Suárez. The approaches for nondestructive inspection and analytical as well as experimental evaluation of criticality, which are currently being used or are being considered for use in the near future, are examined. Acoustic emission appears to be a useful tool for detecting and locating fatigue damage. The effect of notches on static strength is considered to be a phenomenon, for which analytical methods have been validated. Structural testing is considered essential for assessing criticality, but the need for analysis methods to reduce testing costs is emphasized.
9. "Investigation of the Response of Composite Materials by Nondestructive Evaluation" by E. G. Henneke. Use of various NDI techniques are examined and damage accumulation in composites under static and cyclic loading are studied. Attempts to obtain a relationship of characteristic damage states to engineering response are described.

Overviews of sponsored research by the Army, Navy, AFWAL and NASA describing results and objectives of various programs were presented by R. J. Shuford, D. Mulville, G. P. Sendeckyj and G. L. Roderick, respectively. A special topic of interest is the use of a large deformation theory in characterizing delamination growth under compression loads by workers at NASA. General discussions indicate that delamination is the most critical type of defect in composite materials, and in aircraft structural components the critical areas are those where there are sharp changes in geometry like free edges, ply drops, etc. Delaminations created inside a laminate by impact, like tool drops, etc., and those initiated from inherent defects, can also be critical.

DISCUSSION ON STATE OF THE ART

The following is a discussion on the current state of the art of defect criticality assessment as it appears from the literature search and the presentations at the symposium.

Ultrasonic C-scans and Optical as well as Visual Inspection appear to be the most widely used tools for NDI at this point in time. X-ray Radiography and Acoustic Emission have good potentials in this direction. Other techniques like Thermography, Dye Penetrants and Attenuation Measurements are still in the stage of research and development. Very few of the NDI techniques have been shown to yield accurate quantitative measurements of defect size and shape (see B.1.15, 1.17 and MSC TPR 1107/1158). Others are useful for detecting and locating the flaws.

Although various analytical models and criteria have been developed for through-the-thickness defects like cracks or holes and the damage mechanisms which develop under static and cyclic loading are relatively clear, quantitative assessment of criticality of such defects remains a complicated task. The reason for this complexity is the growth of delaminations between various laminae and disbonds in the matrix and/or fiber matrix interfaces in the individual layers. For this reason, use of fracture mechanics methodologies to this problem has met with partial success. Under static loading, use of a stress criterion at a point a little distance away from the cracktip (ref. 5) is considered as a viable method by many investigators as well as in many industries (see presentation by J. A. Suarez in symposium proceedings). Finite element modeling or progressive damage growth modeling as reported by D. Y. Konishi in the symposium may yield more realistic assessments of damage growth, although they have their own limitations, especially from the point of accuracy as well as cost. Modeling of damage growth under cyclic loading is still in the state of research and development (see

bibliography B-1). There exists a strong feeling, however, that tension-tension fatigue is not very critical for fiber composite laminates. Compression fatigue is critical and it appears that delamination growth between the laminae can be modeled by the use of equations similar to the semiempirical crack growth laws commonly used for metals (ref. 4). The usefulness of this approach has been demonstrated, but a considerable amount of groundwork is still to be performed to put the analytical methodology for assessing two-dimensional growth of disbonds starting from the edge of a hole or straight boundary on a sound footing.

Growth of disbonds is an important and, in the opinion of many investigators, the most critical phenomenon, not only in compression fatigue but also in many other circumstances like the one of transverse shear loading, where catastrophic growth can occur under quasi-static loading. Growth of isolated disbonds in Mode I, Mode II or combined modes under quasi-static or cyclic loading has been modeled by various investigators using fracture mechanics methodologies and fatigue crack growth laws (see bibliography B-2). Growth of disbonds from surface flaws or from edges has also been studied. In all such studies, strain energy release rates or stress intensity factors are calculated by analytical/numerical methods, and other semiempirical parameters are determined from correlation with experimental data. In most of these experimental works, the growth of implanted flaws is either one-dimensional or the correlation is attempted via a one-dimensional model. 2-D finite element methods (see B.2.3.6-12) appear to be an attractive tool for numerical calculations because of their versatility to consider various boundary conditions like free edges or surface flaws. The methods, however, can be expensive, especially when their accuracy is investigated by varying mesh sizes and element shapes. No detailed investigation in this direction dealing with laminated composites is reported in literature, although some studies must have been conducted by workers who have used such

techniques. 1-D beam theories (B2.1.4-5, B2.2.2) and 2-D elasticity solutions (B2.2.1), with due consideration to laminate stacking sequence, which have been used for isolated disbonds only, are comparatively inexpensive, but extension of such methods to consideration of disbonds near free edges or surface flaws is complicated and has not yet been attempted. It should be pointed out that techniques of modeling self-similar disbond growth are well advanced, although a significant amount of experimental/analytical correlation studies is needed before they can be used as practical design tools, since, in many cases, the disbond growth is not self similar. Use of 3-D finite elements has also been attempted for calculation of strain energy release rates (see B2.1.7), but very few studies are reported in the literature which deal with two-dimensional growth of disbonds. Obviously, such finite element methods are attractive tools for studying the stress field near disbonds with 2-D planforms, but useful results for such problems have also been obtained by the use of modified laminated plate theories (ref. 3). No study on the use of other 3-D elasticity theories and methods has yet been attempted, but further work in this direction is needed to determine the accuracy of the techniques which are currently in use. Last, but not least, a considerable amount of experimental work is still necessary to determine the various material constants as well as the statistical variability of those parameters which are used in modeling growth of disbonds.

EXPERIMENTAL PROGRAM

The experimental program consisted of the following tasks:

- Task I. Study the effects of changes in disbond position through the thickness of laminated beams on quasi-static propagation.
- Task II. Study the effects of sharpness of the disbond tips on quasi-static failure of thick laminated beams.
- Task III. Growth of disbonds with circular planform under cyclic transverse shear in thick laminated plates.

TASK I. - EFFECTS OF DISBOND LOCATION

Tests were performed on three types of laminates of AS-3501 graphite/epoxy material with seven different defect locations through the thickness of the samples. All tests were performed in three point bending at room temperature.

Test Method

Testing was performed in an Instron load frame at a rate of 1.27 mm (0.05 inches) per minute. Prior to testing, the static test machine was balanced and calibrated and care was taken to assure that the force was introduced perpendicular to, and in the center of, each of the 25.4 mm x 254 mm x 64 ply graphite/epoxy beams. Load was applied using a 12.7 mm dia. circular steel rod and a 12.7 mm wide copper pad for uniform load introduction and to avoid stress concentrations at the center of the beam. Geometry of the test specimens is shown in figure 1. All implanted defects were located in the region of compressive flexural stress. Ultrasonic C-scans were made on all beams prior to testing and if catastrophic failure did not occur after a significant load drop, the beams were rescanned and retested. Examples of these scans are given in figures 2 and 3.

Fabrication and Sample Geometry

Samples were made from AS-3501-6 graphite/epoxy prepreg in three laminate configurations which will be called types A, B and C as follows: Type A = $[0_8/+45_4/-45_4]_{2s}$, Type B = $[0_8/+45_4/-45_4/0_6/+45_4/-45_4/0_2]_s$, Type C = $[0_4/+45_2/-45_2/0_4]_{2s}$. All samples were 64 ply and were fabricated with 25.4 mm x 25.4 mm two ply teflon defects implated in locations described in table 1. Defect location is shown in figure 1 and was verified by the ultrasonic C-scan technique. Samples are identified by the following coded example:

C - 20/21 - 2

Specimen number 2
 Defect location between plies 20 and 21
 Laminate type C = $[0_4/+45_2/-45_2/0_4]_{2s}$

Three replicates for each location were tested which are identified by the specimen number, i.e. the last digit in the example shown above. All samples were cured using the standard cure cycle specified for AS-3501-6 composites. The details of the cure cycle are given below.

1. Prepreg laminate is prepared with bleeder cloths in the ratio of one layer of fiberglass bleeder to three plies of graphite/epoxy.
2. Cool plate is sealed and vacuum is drawn to -30 in. Hg.
3. Temperature is increased to 260°F.
4. Dwell one hour.
5. Pressurize to 85 psi with Nitrogen.
6. Increase temperature to 350°F.
7. Cure at temperature and pressure for two hours.
8. Decrease temperature to below 250° F.
9. Depressurize and cool to room temperature.

Data

All samples were tested until a significant load drop or failure occurred. These data are given for the three laminate configurations in tables 2, 3 and 4. In each table, the following data are given: sample I.D., width, thickness, failure load, defect lengths 1 and 2 (as viewed in the C-scans) and defect spacing. Laminate configurations B and C indicated only one load drop coincident with failure. Laminate type A, however, experienced as many as four load drops prior to failure and these data are given in table 5. After each load drop, the samples were rescanned and tested until the next load drop or failure, as discussed previously.

TASK II. - EFFECTS OF SHARPNESS OF DISBOND TIPS

Test Method

The test method for task II is the same as that for task I. 25.4 mm x 254 mm x 64 ply graphite/epoxy beams with defects implanted between the mid-plyes were loaded in three point bending. The test section was 152.4 mm long and the beams were loaded at the center of the test section. The samples were statically loaded at a rate of 1.27 mm per minute in an Instron load frame. Maximum load was recorded on a chart recorder and later transferred to data tables. Twelve blunt crack specimens and 12 sharp crack specimens were tested.

Fabrication and Sample Geometry

Twelve samples from the test program conducted under contract N62269-79-C-0209, which were 76.2 mm x 254 mm by 64 plies, were used to make the sharp crack specimens. These plates had all been previously fatigued in three point bending. Cyclic loading is known to yield sharp crack fronts. These beams were all ultrasonically C-scanned to determine the sizes and locations of defects. The 76.2 mm wide samples were marked and 25.4 wide beams were cut

from the center region of each plate. These beams were then re-scanned and defect sizes, as well as width and thickness, were measured. These scans and data are given in figure 4 and table 6. Average defect size, radius of the crack front and crack spacing were determined. These data were used to fabricate the blunt crack specimens. The blunt crack specimens were made from AS-3501-6 prepreg and the delaminations were implanted between the center plies of the $[(0_4/\pm 45_2/\mp 45_2/0_4)_5]_5$ laminates. The sample geometry is shown in figure 5, where the defect size and location is indicated. The average defect length was made to be 53.98 mm with a crack front radius of 19.05 mm. The defects were made from two ply teflon as in task I. Specimen identification numbers are prefixed by "B" for blunt as in B-4 and by "S" for sharp as in S-12.

Data

Data are presented in table 6 which contains sample I.D., thickness, width, disbond lengths 1 and 2, maximum load and the defect location at which failure occurred. Ultrasonic C-scans of the blunt and sharp crack specimens are shown in figures 4 and 6, respectively.

TASK III. GROWTH OF CIRCULAR DISBONDS UNDER CYCLIC LOADING

Test Method

Effects of size and location of disbonds placed in $[0_4/\pm 45_2/\mp 45_2/0_4]_{2S}$, AS-3501-6 graphic epoxy laminates on flaw growth under cyclic transverse shear were studied in this task. This was a continuation of the studies on disbonds with 2-D planforms reported in reference 3. Circular disbonds of 25.4 mm, 31.75 mm and 38.1 mm diameter in the form of teflon films were placed in 76.2 mm wide x 254 mm long specimens. Two similar disbonds were

placed symmetrically in the net section span of 152.4 mm with their centers 101.6 mm apart. All fatigue specimens were tested in three point bending in a manner similar to the beam specimens in Task I and II. Some of the disbonds were placed in the mid-plane, i.e. between plies 32/33 and others were placed at $Z=\pm 0.25H$ (between plies 16/17 or 48/49), H being the laminate thickness. It should be pointed out that $Z=+0.25H$ indicates that the disbonds were in the region of compressive flexural stress and $Z=-0.25H$ means that they were in the region of tensile flexural stress.

The samples with 25.4 mm diameter defects were first tested at an S-level of 0.5 based on a static failure load of 29,400 Newtons as determined from tests reported in reference 3. It should be noted that those static failures were due to flexure and not due to transverse shear. The specimens with defects located at $Z=+0.25H$ showed little propagation after 12 million cycles. S-level was, therefore, increased to 0.75 for 31.75 mm and 38.1 mm defects located at $Z=+0.25H$. S-level was kept at 0.5 for all other samples. The ratio R of minimum to maximum load was always kept equal to 0.1. Details of all specimens tested are given in table 7, where measured thicknesses and widths are also given. The specimens are identified according to the scheme given below.

3-1R0-1; 3 refers to task III
 1R refers to 1 inch (25.4 mm) dia. round defect
 0 refers to $Z=0$, midplane
 -1 refers to replicate 1

3-125R-25-2; 125R refers to 1.25 inch (31.75 mm)
 dia. round defect
 -25 refers to $Z=-.25H$
 -2 refers to replicate 2

3-150R+25-3; 150R refers to 1.5 inch (38.1 mm) dia.
 round defect
 +25 refers to $Z=+.25H$
 -3 refers to replicate 3

Data

On an average the 25.4 mm diameter defect samples were scanned about 24 times during their life, while the same figure for 31.75 and 38.1 mm diameter defect samples was about 14. Representative C-scans for some of the samples are given in figures 7-15. Growth of disbands at three locations on four fronts labeled as A, B, C and D (see fig. 16) were measured from each of the scans and the results were tabulated. These data were later used for data correlation studies which are reported in the next section.

DATA CORRELATION STUDIES

Results from tasks I and II were utilized to calculate the critical values of strain energy release rates with the help of the analytical methods developed in reference 2. These methods yield the stress intensity factors and energy release rates at the tips of two symmetrically located disbonds in a laminated composite beam loaded in three point bending. The layers are assumed to be in a state of plane stress. Elastic properties of the layers, nondimensionalized by a factor $E_0 = 6.895 \text{ GPa}$ (10^6 psi) which were used for calculations are given below.

Material	Layers	C_{11}/E_0	C_{33}/E_0	C_{13}/E_0	C_{55}/E_0
1	0°	18.24	1.46	0.409	0.841
2	+45° or -45°	2.16	1.49	0.294	0.711
3	(+45/-45)- smeared	2.88	1.50	0.130	0.687
4	Epoxy Matrix	0.605	0.605	0.228	0.188

TASK I. - EFFECT OF DISBOND LOCATION

Since the +45° and -45° layers are lumped separately in laminate types A and B, properties listed under material no. 2 were used for both of these layers. For consistency, the same properties were also used for laminate C. Calculations indicate that if the properties of a smeared material (no. 3) are used, the results differ by less than five percent.

The computer code DELAM, in its present form, can solve the problem of disbonds between two layers of the same material. In a majority of test specimens, this was the case and 60 nonzero terms of the Fourier Series were enough for the calculation of the regular

kernels of the integral equations. Forty collocation points yielded reasonable accuracy in calculation of the unknown functions, intensity factors and energy release rates. In a few cases, however, the disbonds were between a 0° and a $+45^\circ$ (or a -45°) layer. Although, the code can be modified to handle these cases, this was beyond the scope of the current program. Therefore, calculations were performed for disbonds located between two epoxy matrix layers (material no. 4) of relatively small thicknesses which are sandwiched between 0° and 45° materials. In practice, there is always a matrix rich region between two laminae. Results were obtained for three gradually decreasing values of thickness t_m of the matrix layers (up to $t_m/l = .000734$, l being the span of the beam) and the energy release rates in the limiting case of zero thickness were obtained by extrapolation. A three point extrapolation formula worked well for calculation of G_{II} as it appeared from results of the cases of disbonds between two similar layers. For calculation of G_I , however, the extrapolation procedure was not very satisfactory, especially when the calculated values of G_I were of the order of G_{II} . This phenomenon is expected since the nature of the stress singularity changes from the inverse square root type to the type $-1/2 \pm i\epsilon$, in the limiting case. Moreover, as the thickness of matrix layers is gradually reduced, it is necessary to take increasing number of terms in the Fourier series for calculation of the regular kernels. Three hundred nonzero terms were considered for the smallest thickness. It also appeared that further reduction in the thickness may necessitate the use of more collocation points (>40). For cases where G_I was of the order G_{II} , the values of G_I showed a little oscillatory tendency about an average value. In such cases, the limiting value of G_I was taken as the average of the values calculated for three values of t_m , i.e. $t_m/l = .000734$, $.001468$ and $.002202$ was utilized. Considering the scatter in experimental data, these results appeared satisfactory for the purpose of data correlation studies reported herein.

Calculated values of $G_I E_0 l/P^2$, $G_{II} E_0 l/P^2$, (l = span of the beam and P = applied load per unit width) as well as the total energy release rates are shown in tables 8, 9 and 10 for laminate types A, B and C, respectively. Use of these values and the measured load carrying capacities of the specimens yielded G^C , the critical values of energy release rates, which are also shown in the tables. It should be noted that for laminate types B and C the failure loads were also the maximum loads. Some specimens of type A laminates, however, showed some load drops before final failure occurred as can be seen in table 5. In some cases, i.e., for some of the specimens of the Series A-16/17, A-28/29 and A-32/33, the first load drop occurred at very low loads. The reasons for such load drops before failure are not very clear. It should be pointed out, however, that the present analysis does not consider the effect of the tearing mode (G_{III}), which can have significant influence, especially in cases where the $+45^\circ$ and -45° layers are lumped together. Also, shifting of the disbond location across the thickness of the specimen may yield such load drops. These effects can not be assessed at this time but should be considered in future studies. For the current study, the value of the maximum load was used for calculations. Since the disbond geometry might have changed before the maximum load was attained, the results for laminate type A should be interpreted with some caution.

All calculations were performed for a laminate thickness of 8.95 mm. and a beam width of 25.4 mm. Experimental values of loads were normalized with due consideration to specimen thickness and width and these values are shown in tables 8-10. Considering the scatter of experimental data which exists in results for three test specimens of the same type and values of G_{II}^C reported in table 11 (results of task II discussed in the next subsection), it appears that the critical energy release rate does not vary to a great extent with its location, i.e. the orientation of the layers between which the disbond is located. This is expected if one considers the fact that there is always a matrix rich region between two laminae

and contends that G^C is a characteristic material constant for the matrix material, which may, of course, depend on its type and processing variables.

In a few cases, A-12/13, A-16/17, B-6/7, B-12/13, C-8/9 and C-12/13, calculated values of G_I is of the order of G_{II} and the values of G^C , obtained in these cases are consistently on the low side. This suggests that a quadratic interaction criterion of the type

$$\left(\frac{G_I}{G_I^C}\right)^2 + \left(\frac{G_{II}}{G_{II}^C}\right)^2 = 1 \quad (1)$$

instead of the one used here, $G_I + G_{II} = G^C$, may yield a better fit to the experimental data. If G_{II}^C is taken equal to 1040 N/m (as determined in task II, see table 11), calculations indicate that G_I^C should lie somewhere between 200 to 400 N/m. No detailed examination of such a criterion is attempted here, since the scatter in present data on G_{II}^C does not yield a realistic assessment of G_I^C . Alternative experiments with G_I dominating the response, should be designed for this purpose.

Values of G^C obtained from the specimens of the series B-26/27 are a bit on the high side, reasons for which are not quite clear. In this case, the disbond is located between +45 and -45 and effects of mode III, which is not considered in the analysis, may have something to do with these results. It is noted, however, that other specimens with disbonds between +45 and -45 layers, i.e. B-12/13, A-12/13 and A-28/29 yield values of G^C which are on the low side.

It should be pointed out that in cases when $G_I \neq 0$, the stress intensity factor K_I at one of the tips is positive, whereas at the other tip, it is negative, indicating existence of compressive stresses near that tip. Therefore, it is quite possible that the two surfaces of the disbond may come in contact near such a tip causing frictional resistance. The effect of this phenomenon cannot

be assessed here, but obviously, it may have some influence on the results presented. Tables 8-10 show the location of the tip where K_I was found to be positive. Location c indicates the tip nearer to the supports, and d identifies the tip near the applied load.

To examine the usefulness of the analytical methodology in assessing criticality of disbonds placed at different locations, failure loads P_f for the three types of laminates predicted by the criterion $G = G_I + G_{II} = G^C = 1000 \text{ N/m}$ are plotted in figures 17-19. It may be noted that the criterion yields $P_f^2 = G^C E_0 \ell / \alpha$ where the factor $\alpha = GE_0 \ell / P^2$, listed in tables 8-10. The figures show reasonable correlation with experimental data which have been normalized for 2.54 cm wide beams with 2.54 cm size defects. In general, the differences between predicted and experimental values are higher when contributions of G_I to the total energy release rates are relatively high, indicating that the quadratic interaction criterion discussed earlier or even the assumption of linear interaction with different coefficients associated with G_I and G_{II} may yield better correlation with experimental data.

TASK II. - EFFECT OF SHARPNESS OF DISBOND TIPS

Smearred (+45/-45) material properties (material no. 3) were used for calculation of $G_{II} E_0 \ell / P^2 = GE_0 \ell / P^2$ ($G_I=0$) for disbonds in laminates with a thickness 8.95 mm and a width of 25.4 mm of the type tested in task II. Normalized values of failure loads, with due consideration to width and thickness of the specimens were used for determination of G_{II}^C . Results are given in table 11. Results show some scatter and about 10% difference in average G_{II}^C for blunt and sharp tips. Considering the scatter, this difference is not significant and it appears that the nature of the tip does not have any dominant influence on catastrophic disbond growth under static shear.

TASK III. - PROPAGATION OF DISBOND IN FATIGUE

Strain energy release rates along the periphery of elliptic disbonds of various sizes with semi-axes L_1 and L_2 located at the midsurface of $[0_4/\pm 45_2/\mp 45_2/0_4]_{2s}$ (which can also be written as $[(0_4/\pm 45_2/\mp 45_2/0_4)_s]_s$) AS-3501-6 graphite epoxy laminates were reported in reference 3. These results were also utilized in the present study. Properties of the unidirectionally reinforced composite (0° layer) and stiffness of the $(0_4/\pm 45_2/\mp 45_2/0_4)_s$ laminate are reproduced here in table 12. As indicated in reference 3, D_{16} and D_{26} were neglected for the calculation and the laminate was considered as orthotropic. Since the disbond is located in the mid-plane, the energy release rate G_I in opening mode is identically equal to zero in this case. In the present study, disbonds were also placed at $Z=\pm 0.25H$, H being the laminate thickness. For such location, G_I is nonzero and the variations of G_{II} , G_{III} and G_I along the disbond periphery are shown in figures 20-22. The calculations were performed with laminate properties given in table 13, for self equilibrating uniform shear stress in x-direction on the disbond surfaces. The two laminates were considered orthotropic, i.e. $A_{16}=A_{26}=D_{16}=D_{26}=0$ for the purpose of calculations. As in the case of disbonds in the mid-plane, G_{II} first increases with L_1 and then starts decreasing provided L_2 is kept fixed. Similar behavior is also observed for G_I . Figure 23 shows the variation of G_{II} and G_I at $x = L_1$, $y = 0$ with L_1/L_2 for fixed values of L_1 . It should be noted that in the limiting case $L_1/L_2 \rightarrow 0$, the problem reduces to that of generalized plane strain. Results from the 2-D elasticity solution (ref. 2) for this problem are also shown in the figure. Although the results for this limiting case cannot be obtained by the methods used here, the results indicate that G_{II} is underestimated, as was observed in reference 3 for disbonds in the mid-plane of the laminates. It is clear from

the results given here that G_I is overestimated by the laminated plate theory assumptions. Total energy release rate ($G_I + G_{II}$) is, however, underestimated.

Growth of disbands under cyclic loading observed experimentally were measured and tabulated as described in the previous section. Growth in y direction (in the direction of the width of the plate specimens) was not significant. Growth rates in x-direction were measured at 6 points ($y=0$ and $y=\pm 9.53$ mm). The distance L_1 of the two disband fronts at $y=0$ from the center of each of the two flaws were plotted against N , the number of cycles for each specimen. Some representative data are shown in figures 24-28. Growth rates $\Delta L_1/\Delta N$ were then computed at various points along the L_1 vs. N plots. Values of the current total length of the disband in x-direction were then used as the dimension of the major axis of an approximated elliptic disband to calculate $\Delta(\sqrt{G_{II}})$, the range of variation of $\sqrt{G_{II}}$. Values of dL_1/dN were then plotted against $\Delta(\sqrt{G_{II}})$ on log-log graph papers.

Results for disbands in mid-plane are shown in figure 29. Least square fits were attempted to obtain the empirical constants C_1 and n in the relationship of the form:

$$\frac{dL_1}{dN} = C_1 \{ \Delta(\sqrt{G_{II}}) - \Delta_0(\sqrt{G_{II}}) \}^n \quad (2)$$

A series of values of the threshold range $\Delta_0(\sqrt{G_{II}})$, below which flaw growth is not expected varying between 7 to 11 $(N/m)^{1/2}$ were considered. The constants for two curves which appear to yield good fits are given below in Newton meter units.

$\Delta_0(\sqrt{G_{II}}), (N/m)^{1/2}$	$C_1(N/m \text{ units})$	n
8.0	0.1456×10^{-10}	4.032
10.0	0.2782×10^{-9}	3.095

The curve corresponding to equation (2) with the second set of parameters is shown in figure 29. These parameters differ a little bit from those obtained in reference 3 for disbonds in a similar location, i.e. mid-plane. The difference may be due to difference in mean stress or S values. S values for the specimen tested under the present program were 0.5, whereas for those considered in reference 3, S varied between 0.4 to 0.6. It should also be pointed out that for the maximum load, values of G_{II} attained is of the order of G_{II}^C and, therefore, fitting of curve of the type (2) may not be appropriate for such high values of G_{II} . Curve fits to consider differing S values and high values of G_{II} are currently being attempted in an ongoing follow-on effort.

Results for disbonds located at $Z=\pm 0.25H$ are shown in figure 30 along with the curve fit to data for disbonds at $Z=0$, described above. It is noted that these test data are for two values of S, i.e. $S=0.5$ and $S=0.75$. Since the static failure load was determined from tests which indicated flexural failure and the shear stresses at mid-plane and at $Z=\pm 0.25H$ for a fixed load are not the same, the actual mean stresses for specimens with disbonds in mid-plane and for those with defects at $Z=\pm 0.25H$ could be different. Also, for defects located $Z=\pm 0.25H$, the problem is more complicated because of the existence of G_I , which may increase the flaw growth rate. The values of $\Delta(\sqrt{G_I})$ for these specimens were about half of those of $\Delta(\sqrt{G_{II}})$. An equation to consider simultaneous influence of $\Delta(\sqrt{G_I})$ and $\Delta(\sqrt{G_{II}})$, may be postulated but such an attempt is not made here. It appears, however, that all test data for $S=0.5$ (all of these points be on the left hand side of fitted curve) show a slightly higher growth rate than disbonds at mid-plane. The data points for $S=0.75$ on the other hand fall close to a vertical line indicating a kind of unstable growth pattern, possibly because of the fact the maximum values of G attained in these tests are close to that needed for catastrophic growth under quasi-static loading.

Before closing this discussion, it should be pointed out that growth of a disbond under pure mode II loading should be the same at $x=\pm L_1$ as predicted by the empirical growth law and the stress analysis model used here. The results for beams with mid-plane disbonds, however, show some differences between the growths at the four fronts, possibly because of the presence of inhomogeneities and/or the approximations used in the analysis. This is one of the reasons for the scatter noticed in data correlation. Presence of mixed mode conditions for disbonds at $Z=\pm 0.25H$ may introduce larger differences because of the existence of tensile and compressive normal stresses at the two fronts. As mentioned before, better curve fits to fatigue data are currently being attempted in an ongoing program.

DISCUSSIONS AND CONCLUSIONS

In the present work the state of the art of assessing defect criticality in laminated composites has been summarized and the significance of various ongoing programs in this area have been assessed. In addition, a number of tests have been conducted and data obtained from these tests have been analyzed to test the range of validity of the criticality criteria developed in related past programs. From the results reported herein the following conclusions and comments can be made.

1. A linear elastic fracture mechanics approach and methods of stress analysis based on 2-D elasticity theory can be used to assess criticality of disbonds in laminated beam type structures under transverse shear, irrespective of disbond size and location. Validity of the proposed methodology has been demonstrated for cases where mode II energy release rate is the dominant factor influencing failure. Further work appears necessary to assess the mode III energy release rate as well as the interaction of all three modes; i.e. I, II and III, in causing failure.

2. Sharpness of disbond tips introduced by fatigue loading does not appear to have a significant influence on G_{II}^C , as seen from comparison with test data from disbonds with blunt tips, i.e. implanted teflon defects. However, because of the scatter in experimental results, more tests are needed before a final conclusion is drawn.

3. Methods of stress analysis based on laminated plate theory yield reasonably accurate values of energy release rates along the periphery of disbonds in laminated plate type structures under transverse shear. Usefulness of semi-empirical crack growth laws in predicting the growth of such flaws, for cases where mode II energy release rate is dominant, has been clearly illustrated. Further work for evaluating effects of varying mean stress

as well as influence of mode I and mode II energy release rate on flaw growth are needed to put the NDE methodology for assessing criticality of disbonds under fatigue loading on a sound basis.

REFERENCES

1. Ramkumar, R. L., Kulkarni, S. V., and Pipes, R. B., "Definition and Modeling of Critical Flaws in Graphite Fiber Reinforced Composites," NADC 76228-30, January 1978.
2. Chatterjee, S. N., Hashin, Z., and Pipes, R. B., "Definition and Modeling of Critical Flaws in Graphite Fiber Reinforced Composites," NADC 77278-30, August 1979.
3. Chatterjee, S. N. and Pipes, R. B., "Study of Graphite/Epoxy Composites for Material Flaw Criticality," NADC-78241-60, November 1980.
4. Ratwani, M. M. and Kan, H. P., "Compression Fatigue Analysis of Fiber Composites," NADC 78049-60, September 1979.
5. Nuismer, R. J. and Whitney, J. M., "Uniaxial Failure of Composite Laminates Containing Stress Concentrations," ASTM STP 593, 1975.

BIBLIOGRAPHY B1 - NOTCHED LAMINATES

- 1.1 Carswell, W. S., "Fatigue Damage in Notched Composites," Composites, v. 8, n. 4, October 1977.
- 1.2 Fujii, T., and Maekawa, Z., "Influence of Stress Concentration on Spread of Strength and Fatigue Life in FRP," Zairyo, v. 28, n. 309, June 1979, pp. 504-509.
- 1.3 Habercom, G. E., Jr., "Mathematical Analysis of Stress Cracks, 1977," June 1980, NTIS/PB-80/813447.
- 1.4 Hayashi, I., Togashi, M., Takai, T., and Nakono, M., "Fatigue Fracture Mechanism of GRP Laminates with a Circular Hole," Proc. Jpn. Congr. Mater. Res., 20th, Publ. Soc. of Mater. Sci., Kyoto, Japan, 1977, pp. 232-239.
- 1.5 Karpinskii, D. N., "On the Theory of Fracture of Fibrous Composites," Prob. Prochn., September 1979, pp. 59-62, in Russian.
- 1.6 Kulkarni, S. V., "Engineering Approach to the Prediction of Fatigue Behavior of Unnotched/Notched Fiber Reinforced Composite Laminates," SPI Reinf. Plast. Compos. Inst. Annu. Conf. Proc., 33rd, 1978.
- 1.7 Kulkarni, S. V., McLaughlin, P.V., Jr., Pipes, R. B., and Rosen, B. W., "Fatigue of Notched Fiber Composite Laminates: Analytical and Experimental Evaluation," ASTM STP 617, 1977, pp. 70-92.
- 1.8 Labor, J. D., and Verete, R. M., "Environmentally Controlled Fatigue Tests of Composite Box Beams with Builtin Flaws," J. Aircr., v. 15, n. 5, May 1978, pp. 257-263.
- 1.9 Mandell, J. F., "Fatigue Crack Growth in Fiber Reinforced Plastics," SPI Reinf. Plast. Compos. Inst. Annu. Conf. Proc., 34th, 1979.
- 1.10 McGarry, F. J., Rowe, E. H., and Riew, C. K., "Improving the Crack Resistance of BMC and SMC," SPI Reinf. Plast. Compos. Inst. Annu. Conf. Proc., 32nd, 1977.
- 1.11 Panasyuk, V. V., "Propagation of Cracks in Composite Materials," NASA-TT-F-13934, Translation from Fiz.-Khim. Mekh. Mater., USSR, v. 7, n. 1, 1971, pp. 108-110.
- 1.12 Pipes, R. B., Kulkarni, S. V., and McLaughlin, P. V., Jr., "Fatigue Damage in Notched Fiber Composites," Mater. Sci. Eng. (Switzerland), v. 30, n. 2, October 1977, pp. 113-120.

BIBLIOGRAPHY B1 - NOTCHED LAMINATES (Continued)

- 1.13 Regel, V. R., and Tamuzh, V. P., "Fracture and Fatigue of Polymers and Composites (Survey)," Mekh. Polym. (USSR), Transl. in Polym. Mekh. (USA), v. 13, n. 3, May-June 1977, pp. 392-408.
- 1.14 Rowlands, R. E., and Stone, E. L., "Application of Experimental Methods to Fracture of Composites," in Proc. of the First USA-USSR Symp. of Fract. of Comp. Mater., 1979, Sijthoff and Noordhoff, Netherlands, pp. 361-371.
- 1.15 Sendeckyj, G. P., Maddux, G. E., and Tracey, N. A., "Comparison of Holographic, Radiographic and Ultrasonic, Techniques for Damage Detection in Composite Materials," Proc. of the Int. Conf. on Compos. Mater., 2nd (ICCM2), Publication of Metall. Soc. of AIME, 1978, pp. 1037-1056.
- 1.16 Stinchcomb, W. W., and Reifsnider, K. L., "Fatigue Damage Mechanisms in Composite Materials: A Review," ASTM STP, 1979, Fatigue Mechanisms, Kansas City, Mo., May 1978.
- 1.17 Sturgeon, J. B., "Fatigue Mechanisms, Characterization, Defects and Their Detection in Reinforced Plastic Materials," Br. J. Non. Destr. Test. v. 20, n. 6, November 1978, pp. 303-310.
- 1.18 Suzuki, M., and Iwamoto, M., "Effect of Mean Stress on Fatigue Crack Propagation in Fiber Reinforced Polycarbonates," Zairyo, v. 28, n. 306, March 1979, pp. 230-236.
- 1.19 Thert, W. G. J., "Residual Strength of Multiply Carbon-Epoxy Kevlar-Epoxy Notched Laminates," Presented at the 14th Intern. AAAF Aeron. Cong. on New Development in Struct. & Mater., Paris, April 1979.
- 1.20 White, M. K., and Wright, M. A., "The Fatigue Properties of Cross-Plied Boron 6061 Aluminum," J. Mater. Sci., (GB), vol. 14, n. 3, March 1979, pp. 653-662.
- 1.21 Young P. C., Stinchcomb, W. W., and Reifsnider, K. L., "Characterization of Constraint Effects on Flaw Growth," ASTM STP 696, 1979, pp. 316-338.

BIBLIOGRAPHY B2 - DELAMINATIONS

2.1 MODE I DELAMINATIONS

- 2.1.1 Bascom, W. D., Bitner, J. L., Moulton, R. J., and Siebert, A. R., "The Interlaminar Fracture of Organic-Matrix, Woven Reinforcement Composites," Composites Journal, 1980, pp. 9-18.
- 2.1.2 de Charentenay, F. X., Bethmont, M., Benzeggah, M., and Chrétien, J. F., "Delamination of Glass Fiber Reinforced Polyester, An Acoustic Emission Study," Proceedings of ICM3, vol. 3, Cambridge, England, August 1979.
- 2.1.3 de Charentenay, F. X., and Benzeggagh, M., "Fracture Mechanics of Mode I Delamination in Composite Materials," Proceedings of ICCM3, Paris, France, August 1980.
- 2.1.4 Devitt, D. F., "Delamination Fracture Toughness of a Unidirectional Composite," M.S. Thesis, Texas A&M University, 1979.
- 2.1.5 Devitt, D. F., Schapery, R. A., and Bradley, W. L., "A Method for Determining the Mode I Delamination Fracture Toughness of Elastic and Viscoelastic Composite Materials," Jr. of Composite Materials, v. 14, October 1980, pp. 270-285.
- 2.1.6 Miller, A. G., Hertzberg, P. E., and Ranatala, V. W., "Toughness Testing of Composite Materials," Proceedings of the Twelfth National Sampe Technical Conference, Seattle, Washington, October 1980, p. 279.
- 2.1.7 Wilkins, D. J., Eisenmann, J. R., Camin, R. A., Margolis, B. S., and Benson, R. A., "Characterizing Delamination Growth in Graphite-Epoxy," Presented at the ASTM Symposium on Composites Damage Tolerance in Miami, November 1980.

2.2 MODE II DELAMINATIONS

- 2.2.1 Chatterjee, S. N., Hashin, Z., and Pipes, R. B., "Definition and Modeling of Critical Flaws in Graphite Fiber Reinforced Resin Matrix Composite Materials," NADC-77278-30, Warminster, Pa., August 1979.
- 2.2.2 Ramkumar, R. L., Kulkarni, S. V., and Pipes, R. B., "Definition and Modeling of Critical Flaws in Graphite Fiber Reinforced Epoxy Resin Matrix Composite Materials," NADC-76228-30, Warminster, Pa., January 1978.

BIBLIOGRAPHY B2 - DELAMINATIONS (Continued)

2.3 COMBINED MODE EFFECTS

- 2.3.1 Crossman, F. W., Warren, W. J., Wang, A. S. D., and Law, G. E., "Initiation and Growth of Transverse Cracks and Edge Delamination in Composite Laminates, Part 2. Experimental Correlation," Drexel University, Phila., Pa., 1979.
- 2.3.2 Im, J., Mandell, J. E., Wang, S. S., and McGarry, F. J., "Surface Crack Growth in Fiber Composites," NASA-CR-135094, 1976.
- 2.3.3 Reifsnider, K. L., Henneke, E. G., and Stinchcomb, W. W., "Delamination of Quasi-Isotropic Graphite-Epoxy Laminates," Composite Materials: Testing and Design, ASTM STP 617, 1977, p. 93.
- 2.3.4 Rybicki, E. F., Schmueser, D. W., and Fox, J., "An Energy Release Rate Approach for Stable Crack Growth in the Free Edge Delamination Problem," Journal of Composite Materials, v. 11, 1977, p. 470.
- 2.3.5 Stalnaker, D. O., and Stinchcomb, W. W., "Load History - Edge Damage Studies in Two Quasi-Isotropic Graphite-Epoxy Laminates," ASTM STP 674, 1978, pp. 620-641.
- 2.3.6 Wang, A. S. D., "On Free-Edge Delamination in Laminated Composites," Drexel University, Phila., Pa., 1978.
- 2.3.7 Wang, A. S. D., and Crossman, F. W., "Initiation and Growth of Transverse Cracks and Edge Delamination in Composite Laminates: Part 1. An Energy Method," Drexel University, Phila., Pa., 1979.
- 2.3.8 Wang, S. S., "An Analysis of Delamination in Angle-Ply Fiber-Reinforced Composites," ASME Journal of Applied Mechanics, v. 47, 1980, pp. 64-70.
- 2.3.9 Wang, S. S., "Delamination Crack Growth in Unidirectional Fiber-Reinforced Composites Under Static and Cyclic Loading," Composite Materials: Testing and Design (Fifth Conference), ASTM STP 674, 1979, pp. 642-663.
- 2.3.10 Wang, S. S., "Delamination Fracture From Surface Notch in [(+45°)/0°/90°] Graphite/Epoxy Composites," Proceedings of the Second International Conference on Composite Materials, (ICCM-II) TMS-AIME 1978, pp. 277-291.

BIBLIOGRAPHY B2 - DELAMINATIONS (Continued)

- 2.3.11 Wang, S. S., and Mandell, J. F., "Analysis of Delamination in Unidirectional and Crossplied Fiber-Reinforced Composites Containing Surface Cracks," NASA-CR-135248, 1977.
- 2.3.12 Wang, S. S., and Wang, H. T., "Interlaminar Crack Growth in Fiber-Reinforced Composites During Fatigue," ASME Journal of Engineering Materials and Technology, v. 101, 1979, pp. 34-41.
- 2.3.13 Williams, R. S., and Reifsnider, K. L., "Strain Energy Release Rate Method for Predicting Failure Modes in Composite Materials," ASTM-STP 677, 1978, pp. 629-650.
- 2.4 FATIGUE AND COMPRESSION LOADS
- 2.4.1 Byers, B. A., McCarty, J. E., and Stoecklin, R. L., "Behavior of Damaged Graphite/Epoxy Laminates Under Compression Loading," NASA Special Review of ACEE Composites Programs, Pasadena, California, 20 March 1979.
- 2.4.2 Konishi, D. Y., and Johnston, W. R., "Fatigue Effects on Delaminations and Strength Degradation in Graphite-Epoxy Laminates," ASTM STP 674, 1978, pp. 597-619.
- 2.4.3 Parker, D. E., "Development of Low-Cost Composite Vertical Stabilizer, Vol. II, Proofloading Methodology," Technical Report AFFDL-TR-78-5, Air Force Materials Laboratory, Dayton, Ohio, 9 June 1978.
- 2.4.4 Ratwani, M. M., and Kan, H. P., "Compression Fatigue Analysis of Fiber Composites," NADC-78049-60, Naval Air Development Center, Warminster, Pa., September 1979.
- 2.4.5 Roderick, G. L., Everett, R. A., and Crews, J. H., Jr., "Debond Propagation in Composite-Reinforced Metals," Fatigue of Composite Materials, ASTM STP 569, 1975, pp. 295-306.
- 2.4.6 Roderick, G. L., Everett, R. A., and Crews, J. H., Jr., "Cyclic Debonding of Unidirectional Composite Bonded to Aluminum Sheet for Constant-Amplitude Loading," NASA TN D-8126, 1976.
- 2.4.7 Sendekyj, G. P., Stalnaker, H. D., and Kleismit, R. A., "Effect of Temperature on Fatigue Response of Surface-Notched [(0/±45/0)_s]₃ Graphite-Epoxy Laminate," Fatigue of Filamentary Composite Materials, ASTM STP 636, 1977, pp. 123-140.

BIBLIOGRAPHY B2 - DELAMINATIONS (Concluded)

- 2.4.8 Tarnopolskii, Y. M., Khitrov, V. V., Shomsurin, M. W., and Vasilevskii, V. M., "Debonding Risk for Short Metal-Clad Composite Compression Members," Mekh. Polim. (USSR), Transl. in Polym. Mekh. (USA), v. 14, n. 1, January-February 1978, pp. 22-27.
- 2.4.9 Wagoner, G., and Erbacher, H., "Damage Tolerance Program for the B-1 Composite Stabilizer," Proceedings of the AIAA Conference on Aircraft Composites: The Emerging Methodology for Structural Assurance, San Diego, Ca., 24-25 March 1977.
- 2.4.10 Wolff, R. V., and Wilkins, D. J., "Life Assurance of Composite Structures," Third Conference on Fibrous Composites in Flight Vehicle Design, Williamsburg, Va., 4-6 November 1975, NASA TMX-3377, 1976, pp. 779-802.
- 2.4.11 Wolff, R. V., and Wilkins, D. J., "Durability Evaluation of Highly Stressed Wing Box Structure," Fourth Conference on Fibrous Composites in Structural Design, San Diego, Ca., 14-17 November 1978.

Table 1. Laminate Type and Defect Location - Task I:
Effect of Delamination Location on Criticality

A	B	C
$[0_8/+45_4/-45_4]_{2s}$	$[0_8/+45_4/-45_4/0_6/+45_4$ $-45_4/0_2]_s$	$[0_4/+45_2/-45_2/0_4]_{2s}$
<p>No Defect</p> <p>8/9</p> <p>12/13</p> <p>16/17</p> <p>20/21</p> <p>24/25</p> <p>28/29</p> <p>32/33</p>	<p>No Defect</p> <p>6/7</p> <p>12/13</p> <p>20/21</p> <p>26/27</p> <p>28/29</p> <p>30/31</p> <p>32/33</p>	<p>No Defect</p> <p>8/9</p> <p>12/13</p> <p>16/17</p> <p>20/21</p> <p>24/25</p> <p>28/29</p> <p>32/33</p>

Table 2. Test Data for Type A Laminates - Task I

Sample/ Delam. Location	Thickness mm	Width mm	Failure Load Newtons	Defect Length, mm	Defect Spacing mm
				1	2
A-0/0-1	8.55	25.30	10,288	No Defect	--
-2	8.40	25.17	8,622	No Defect	--
-3	8.79	25.40	10,876	No Defect	--
A-9/9-1	8.81	25.22	7,280	26.92	27.69
-2	9.07	25.30	6,594	27.69	26.92
-3	9.04	25.43	6,584	27.69	26.92
A-12/13-1	9.04	25.60	5,781	27.69	26.16
-2	9.04	25.58	5,536	26.16	26.16
-3	8.99	25.30	5,487	25.40	27.69
A-16/17-1	8.76	25.40	5,350	27.69	26.92
-2	8.61	25.37	5,977	27.69	26.16
-3	8.36	25.50	6,075	26.16	26.92
A-20/21-1	8.99	25.53	6,663	25.40	25.40
-2	8.71	25.50	6,614	26.16	25.40
-3	8.48	25.35	6,222	26.16	26.16
A-24/25-1	9.42	25.27	3,184	25.40	26.16
-2	8.97	25.35	3,135	26.16	26.16
-3	9.30	25.43	3,037	26.16	25.40
A-28/29-1	9.07	25.40	3,135	26.92	25.40
-2	9.22	25.35	3,135	26.16	25.40
-3	9.40	25.48	3,380	26.92	26.16
A-32/33-1	8.66	25.45	2,694	26.16	27.69
-2	8.79	25.35	3,184	26.92	26.16
-3	8.81	25.35	3,086	26.92	26.92

Table 3. Test Data for Type B Laminates - Task I

Sample/ Delam. Location	Thickness mm	Width mm	Failure Load Newtons	Defect Length, mm	Defect Spacing mm
				1	2
B-6/7-1	8.43	25.30	8,622	28.70	27.69
-2	8.64	25.35	8,622	28.70	27.69
-3	8.84	25.30	--	28.70	27.69
B-12/13-1	9.04	25.40	6,859	27.69	27.69
-2	9.14	25.53	7,918	26.92	26.92
-3	9.14	25.50	6,859	26.92	27.69
B-20/21-1	8.46	25.48	5,291	26.92	26.92
-2	9.17	25.45	5,487	26.92	27.69
-3	9.12	25.32	5,291	27.69	26.92
B-26/27-1	8.97	25.60	7,055	26.92	27.69
-2	8.92	25.48	6,614	27.69	27.69
-3	8.94	25.48	7,025	27.69	26.92
B-28/29-1	8.86	25.62	5,213	26.92	27.69
-2	8.99	25.62	5,242	26.92	26.92
-3	9.12	25.62	5,017	27.69	26.16
B-30/31-1	9.22	25.35	5,712	26.16	25.40
-2	9.22	25.48	5,585	26.92	26.16
-3	9.19	25.43	5,438	26.92	26.92
B-32/33-1	9.22	25.35	6,908	26.16	26.16
-2	9.22	25.35	6,761	26.16	25.40
-3	9.19	25.48	5,663	26.16	25.40
B-0/0-1	8.84	25.37	10,190	No Defect	--
-2	8.69	25.43	10,384	No Defect	--
-3	8.46	25.48	11,169	No Defect	--

Table 4. Test Data for Type C Laminates - Task I

Sample/ Delam. Location	Thickness mm	Width mm	Failure Load Newtons	Defect Length, mm	Defect Spacing mm
			1	2	
C-0/0-1	8.43	25.50	8,671	No Defect	--
-2	8.31	25.60	8,524	No Defect	--
-3	8.10	24.94	8,475	No Defect	--
C-8/9-1	8.41	25.30	8,132	26.92	73.91
-2	8.36	25.40	7,721	28.70	73.91
-3	8.33	25.35	7,691	26.16	74.68
C-12/13-1	8.48	25.35	7,819	28.70	73.91
-2	8.61	25.50	8,524	28.70	73.91
-3	8.69	25.48	9,504	29.46	72.14
C-16/17-1	8.69	25.76	8,740	27.69	73.91
-2	8.59	25.40	8,524	26.92	73.91
-3	8.66	25.50	7,544	27.69	73.91
C-20/21-1	8.97	25.30	6,188	25.40	75.44
-2	9.25	25.35	6,365	25.40	76.20
-3	9.47	25.40	6,375	24.64	76.20
C-24/25-1	9.75	25.53	6,865	25.40	76.20
-2	9.80	25.50	6,865	25.40	76.96
-3	9.83	25.27	6,345	25.40	76.96
C-28/29-1	9.68	25.35	6,276	24.64	76.20
-2	9.58	25.37	6,271	24.64	76.20
-3	9.42	25.37	5,796	24.64	76.20
C-32/33-1	9.09	25.50	6,423	25.40	76.20
-2	9.09	25.43	6,845	25.40	76.20
-3	8.89	25.98	6,080	25.40	75.44

Table 5. Load Drop Data for Type A Laminates - Task I

Specimen	Load at First Drop Newtons	Load at Second Drop Newtons	Load at Third Drop Newtons	Failure Load Newtons
A-8/9-1	--	--	--	7,280
-2	--	--	--	6,594
-3	6,271	--	--	6,584
A-12/13-1	3,282	4,556	5,242	5,781
-2	4,821	--	--	5,536
-3	4,899	--	--	5,487
A-16/17-1	--	--	--	5,350
-2	2,136	4,703	6,026	5,977
-3	2,244	--	--	6,075
A-20/21-1	--	--	--	6,663
-2	--	--	--	6,614
-3	--	--	--	6,222
A-24/25-1	3,184	4,899	--	3,184
-2	3,282	4,772	--	3,135
-3	3,380	4,850	--	3,037
A-28/29-1	892	3,723	2,939	3,135
-2	1,322	3,674	2,743	3,135
-3	1,519	3,919	3,086	3,380
A-32/33-1	1,685	3,968	2,841	2,694
-2	2,058	4,037	2,939	3,184
-3	2,254	4,213	3,282	3,086

Table 6. Test Data for Blunt (B) and Sharp (S) Delaminations - Task II

Sample	Thickness mm	Width mm	Max. Load Newtons	Disbond Length, mm		Failure of Disbond
				1	2	
B-1	8.28	25.58	3,729	52.40	53.98	1
-2	8.92	25.58	3,444	53.19	52.40	1
-3	9.02	25.53	3,557	53.98	53.98	1
-4	9.02	25.45	3,675	53.19	53.98	1
-6	8.94	25.53	3,376	53.19	53.19	1
-7	8.66	25.58	3,454	53.98	53.98	1
-9	8.36	25.58	3,307	53.98	53.98	1
-10	8.81	25.73	3,307	53.98	53.98	1
-11	8.20	25.32	2,797	53.19	53.98	2
-12	8.31	25.32	2,492	53.98	53.98	1
-13	8.56	25.37	2,895	53.98	54.76	1
-14	8.74	25.48	2,699	54.76	53.98	1
S-3	9.53	25.37	2,851	53.98	58.75	2
-4	9.86	25.40	3,263	55.58	50.80	1
-5	9.45	25.37	2,988	60.33	57.15	1
-6	9.40	25.37	2,919	68.28	68.28	1
-10	9.70	25.35	2,846	66.68	56.36	2
-12	9.32	25.35	5,790	27.00	33.35	2
-13	9.63	25.40	3,199	42.88	52.40	2
-14	9.78	25.35	3,778	44.45	46.84	1
-15	9.83	25.35	3,214	61.93	59.54	2
-16	9.42	25.35	3,278	55.58	60.33	2
-17	9.45	25.35	3,190	54.76	52.40	1
-18	9.37	25.35	2,846	61.11	61.93	2

Table 7. Details of Samples with Circular Disbonds
Tested in Fatigue - Task III

Sample	S-Level	Max. No. of Cycles, 10^3	Thickness, mm.	Width, mm.
3-1R0-1	.5	380	9.68	76.0
-2		520	9.14	74.5
-4		210	8.84	75.8
3-1R+25-1	.5	2,952	9.53	76.0
-2		11,345	9.19	76.4
-3		750	9.50	75.9
3-1R-25-1	.5	290	8.31	75.9
-2		680	8.66	76.3
-3		940	8.74	76.3
3-125R0-1	.5	36	8.79	75.6
-2		28	8.64	76.0
-3		16	8.31	75.7
3-125R+25-1	.75	27.5	8.59	75.9
-2		5.55	8.28	75.8
3-125R-25-1	.5	32	9.75	76.0
-2		32	9.70	76.4
-3		30.5	8.92	76.3
3-150R0-1	.5	7	7.59	75.3
-2		14.77	8.26	74.9
-3		15	8.28	75.8
3-150R+25-1	.75	4.61	8.61	75.1
-2		12.5	8.69	75.6
-3		6	8.92	75.7

Table 7. Details of Samples with Circular Disbonds (continued)
Tested in Fatigue - Task III

Sample	S-Level	Max. No. of Cycles, 10^3	Thickness, mm.	Width, mm.
3-150R-25-1	.5	18	8.31	74.0
-2		18	8.36	75.6
-3		16	9.68	76.4

Table 8. Data Correlation for Type A Laminates - Task I

Sample	Interface	Normalized Max. Load, Newtons	$G_I E_0 \ell / P^2$	$G_{II} E_0 \ell / P^2$	$G E_0 \ell / P^2$	Location	G_N / m
A-8/9-1		7,445	0.69	3.0	8.7	c	711
-2	0/45	6,535	0.69	8.0	8.7		548
-3		6,511	0.69	8.0	8.7		544
A-12/13-1		5,677	2.35	7.37	9.7	c	462
-2	+45/-45	5,442	2.10	6.82	8.9		390
-3		5,484	2.35	7.37	9.7		431
A-16/17-1		5,465	3.5	6.8	10.3	c	454
-2	-45/0	6,270	3.5	6.8	10.3		597
-3		6,481	3.3	6.6	9.9		613
A-20/21-1		6,600	0.40	11.31	11.7	c	752
-2	0/0	6,768	0.44	11.88	12.3		832
-3		6,578	0.44	11.88	12.3		786
A-24/25-1		4,677	0.57	26.4	27.0	d	871
-2	0/+45	4,774	0.57	26.4	27.0		908
-3		4,666	0.57	26.4	27.0		867
A-28/29-1		3,675	.04	31.41	31.5	d	627
-2	+45/-45	3,574	.03	29.99	30.0		566
-3		3,722	.04	31.41	31.5		643

Table 8. Data Correlation for Type A Laminates - Task I (continued)

Sample	Interface	Normalized Max. Load, Newtons	$G_I E_0^2 / P^2$	$G_{II} E_0^2 / P^2$	$G E_0^2 / P^2$	Location	$G^C N/m$
A-32/33-1		4,093	0	34.21	34.2	c, d	845
-2	-45/-45	4,119	0	32.69	32.7		818
-3		4,287	0	32.69	32.7		886

Table 9. Data Correlation for Type B Laminates - Task I

Sample	Interface	Normalized Max. Load, Newtons	$G_{I E_0} \ell / P^2$	$G_{II E_0} \ell / P^2$	$GE_0 \ell / P^2$	Location	$G_c^c N/m$
B-6/7-1		9,189	1.00	3.76	4.76	c	593
-2	0/0	8,954	1.00	3.76	4.76		563
-3		--	1.00	3.76	4.76		--
B-12/13-1		6,790	2.46	7.81	10.27	c	698
-2	+45/-45	7,712	2.33	7.51	9.84		863
-3		6,687	2.46	7.81	10.27		677
B-20/21-1		5,582	0.41	13.87	14.28	c	656
-2	0/0	5,346	0.45	14.54	14.99		632
-3		5,209	0.45	14.54	14.99		600
B-26/27-1		6,987	0.34	24.08	24.42	c	1,759
-2	+45/-45	6,621	0.34	24.08	24.42		1,579
-3		7,012	0.34	24.08	24.42		1,771
B-28/29-1		5,217	0.73	23.93	24.66	c	990
-2		5,172	0.68	22.88	23.56		930
-3		4,881	0.73	23.93	24.66		867
B-30/31-1		5,556	1.44	21.0	22.4	c, d	1,020
-2	-45/0	5,406	1.54	22.5	24.0		1,035
-3		5,288	1.54	22.5	24.0		990

Table 9. Data Correlation for Type B Laminates - Task I (continued)

Sample	Interface	Normalized Max. Load, Newtons	$G_I E_0 \ell / p^2$	$G_{II} E_0 \ell / p^2$	$GE_0 \ell / p^2$	Location	$G_c N / m$
B-32/33-1		6,720	0	19.00	19.00	c, d	1,266
	-2	6,577	0	19.00	19.00		1,212
	-3	5,496	0	19.00	19.00		847

Table 10. Data Correlation for Type C Laminates - Task I

Sample	Interface	Normalized Max. Load, Newtons	$G_{IE_0} \ell/p^2$	$G_{II_0} \ell/p^2$	$GE_0 \ell/p^2$	Location	G_N/m
C-8/9-1		8,693	1.98	3.46	5.44	c	606
-2	-45/+45	8,270	1.98	3.46	5.44		549
-3		8,280	1.85	3.29	5.14		520
C-12/13-1		8,266	2.9	3.4	6.3	c	635
-2	+45/0	8,826	2.9	3.4	6.3		724
-3		9,764	2.9	3.4	6.3		886
C-16/17-1		8,881	0.69	9.13	9.82	c	1,143
-2	0/0	8,887	0.69	9.13	9.82		1,144
-3		7,766	0.69	9.13	9.82		874
C-20/21-1		6,202	0	19.0	19.0	c	1,078
-2	0/+45	6,175	0	19.0	19.0		1,069
-3		6,023	0	19.0	19.0		1,017
C-24/25-1		6,269	0.53	19.12	19.65	c	1,139
-2	-45/-45	6,242	0.53	19.12	19.65		1,129
-3		5,807	0.53	19.12	19.65		977
C-28/29-1		5,817	2.03	18.5	20.5	c	1,023
-2	+45/0	5,868	1.85	17.7	19.6		996
-3		5,511	2.03	18.5	20.5		918

Table 10. Data Correlation for Type C Laminates - Task I (continued)

Sample	Interface	Normalized Max. Load, Newtons	$G_{I}E_0 \mu/P^2$	$G_{II}E_0 \mu/P^2$	$GE_0 \mu/P^2$	Location	G^C_N/m
C-32/33-1		6,297	0	17.27	17.27	c, d	1,010
-2	0/0	6,731	0	18.17	18.17		1,214
-3		5,984	0	17.27	17.27		912

Table 11. Calculated Values of Critical Energy Release Rates for Blunt and Sharp Tips

Blunt				Sharp			
Sample	Norm. Max. Load, Newtons	$G_{II} E_0 \ell / P^2$	$G_{II}^C, N/m$	Sample	Norm. Max. Load, Newtons	$G_{II} E_0 \ell / P^2$	$G_{II}^C, N/m$
B-1	4,003	61.23	1,447	S-3	2,681	76.16	807
B-2	3,434	62.96	1,095	S-4	2,964	68.43	887
B-3	3,514	64.72	1,179	S-5	2,833	80.29	951
B-4	3,641	62.96	1,231	S-6	2,783	110.1	1,258
B-6	3,363	62.96	1,050	S-10	2,630	70.38	718
B-7	3,545	64.72	1,200	S-12	5,570	26.61	1,218
B-9	3,316	64.72	1,050	S-13	2,975	61.23	799
B-10	3,315	64.72	1,049	S-14	3,465	44.94	796
B-11	3,060	64.72	894	S-15	2,932	78.18	991
B-12	2,694	64.72	693	S-16	3,119	80.29	1,152
B-13	3,030	64.72	876	S-17	3,028	66.46	899
B-14	2,756	66.46	745	S-18	2,723	84.85	928
		Average	1,042+214		Average	950+175	

Table 12. Elastic Properties of 0° Layer and Stiffnesses of $(0_4/\pm 45_2/\mp 45_2/0_4)_s$ Laminate

Transversely Isotropic 0° Layer

$$E_A = 125 \text{ GPa}$$

$$E_T = 10 \text{ GPa}$$

$$\nu_A = 0.28$$

$$G_A = 5.8 \text{ GPa}$$

$(0_4/\pm 45_2/\mp 45_2/0_4)_s$ Laminate

$$A_{11} = 4.06 \times 10^8 \text{ N/m.}$$

$$D_{11} = 877 \text{ Nm.}$$

$$A_{12} = 0.79 \times 10^8 \text{ N/m.}$$

$$D_{12} = 131 \text{ Nm.}$$

$$A_{22} = 1.24 \times 10^8 \text{ N/m.}$$

$$D_{22} = 218 \text{ Nm.}$$

$$A_{66} = 0.95 \times 10^8 \text{ N/m.}$$

$$D_{66} = 160 \text{ Nm.}$$

$$A_{16} = A_{26} = 0.0$$

$$D_{16} = D_{26} = 3.25 \text{ Nm.}$$

$$B_{\alpha\beta} = 0.0 \quad (\alpha, \beta = 1, 2, 6)$$

$$K_{55} = 2.12 \times 10^7 \text{ N/m.}$$

$$K_{44} = 1.75 \times 10^7 \text{ N/m.}$$

Ply Thickness = 0.1519 mm.

Table 13. Stiffnesses of $(0_4/+45_2/-45_2/0_4)$ and $(0_4/+45_2/-45_2/0_4)_3$ Laminates

$(0_4/+45_2/-45_2/0_4)$

$$\begin{aligned} A_{11} &= 2.03 \times 10^8 \text{ N/m} & D_{11} &= 138 \text{ Nm} \\ A_{12} &= 0.394 \times 10^8 \text{ N/m} & D_{12} &= 7.4 \text{ Nm} \\ A_{22} &= 0.623 \times 10^8 \text{ N/m} & D_{22} &= 16.7 \text{ Nm} \\ A_{66} &= 0.466 \times 10^8 \text{ N/m} & D_{66} &= 11.0 \text{ Nm} \\ A_{16} &= A_{26} = 0 & D_{16} &= D_{26} = 1.63 \text{ Nm} \end{aligned}$$

$$B_{\alpha\beta} = 0 \quad (\alpha, \beta = 1, 2, 6)$$

$$K_{ss} = 1.06 \times 10^7 \text{ N/m} \quad K_{44} = 0.875 \times 10^7 \text{ N/m}$$

$(0_4/+45_2/-45_2/0_4)_3$

$$\begin{aligned} A_{11} &= 6.09 \times 10^8 \text{ N/m} & D_{11} &= 2817 \text{ Nm} \\ A_{12} &= 1.18 \times 10^8 \text{ N/m} & D_{12} &= 488 \text{ Nm} \\ A_{22} &= 1.87 \times 10^8 \text{ N/m} & D_{22} &= 787 \text{ Nm} \\ A_{66} &= 1.40 \times 10^8 \text{ N/m} & D_{66} &= 585 \text{ Nm} \\ A_{16} &= A_{26} = 0 & D_{16} &= D_{26} = 1.63 \text{ Nm} \end{aligned}$$

$$B_{\alpha\beta} = 0 \quad (\alpha, \beta = 1, 2, 6)$$

$$K_{55} = 3.18 \times 10^7 \text{ N/m} \quad K_{44} = 2.63 \times 10^7 \text{ N/m}$$

Ply thickness = 0.1519 mm

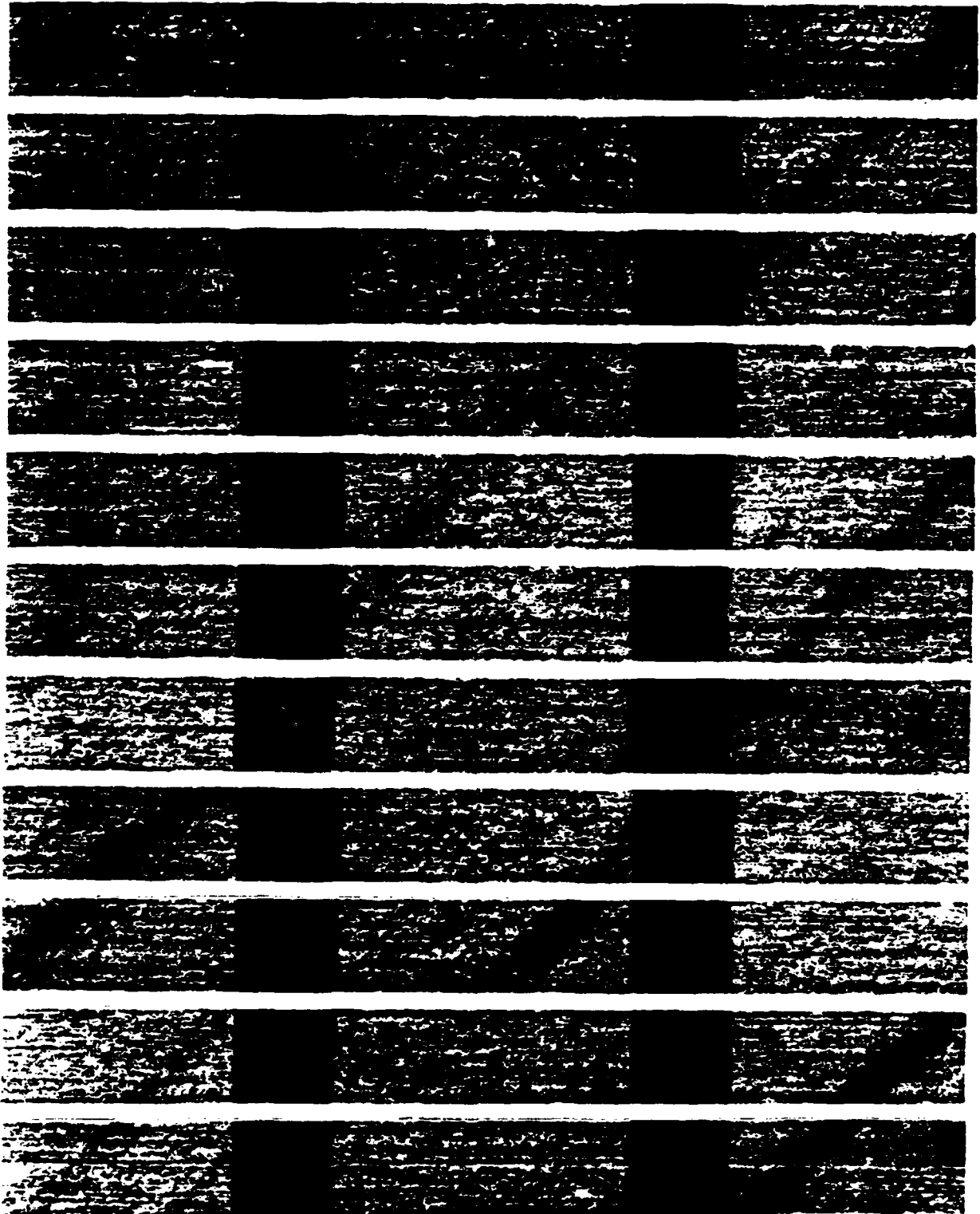


Figure 2. Representative C-scans Prior to Loading

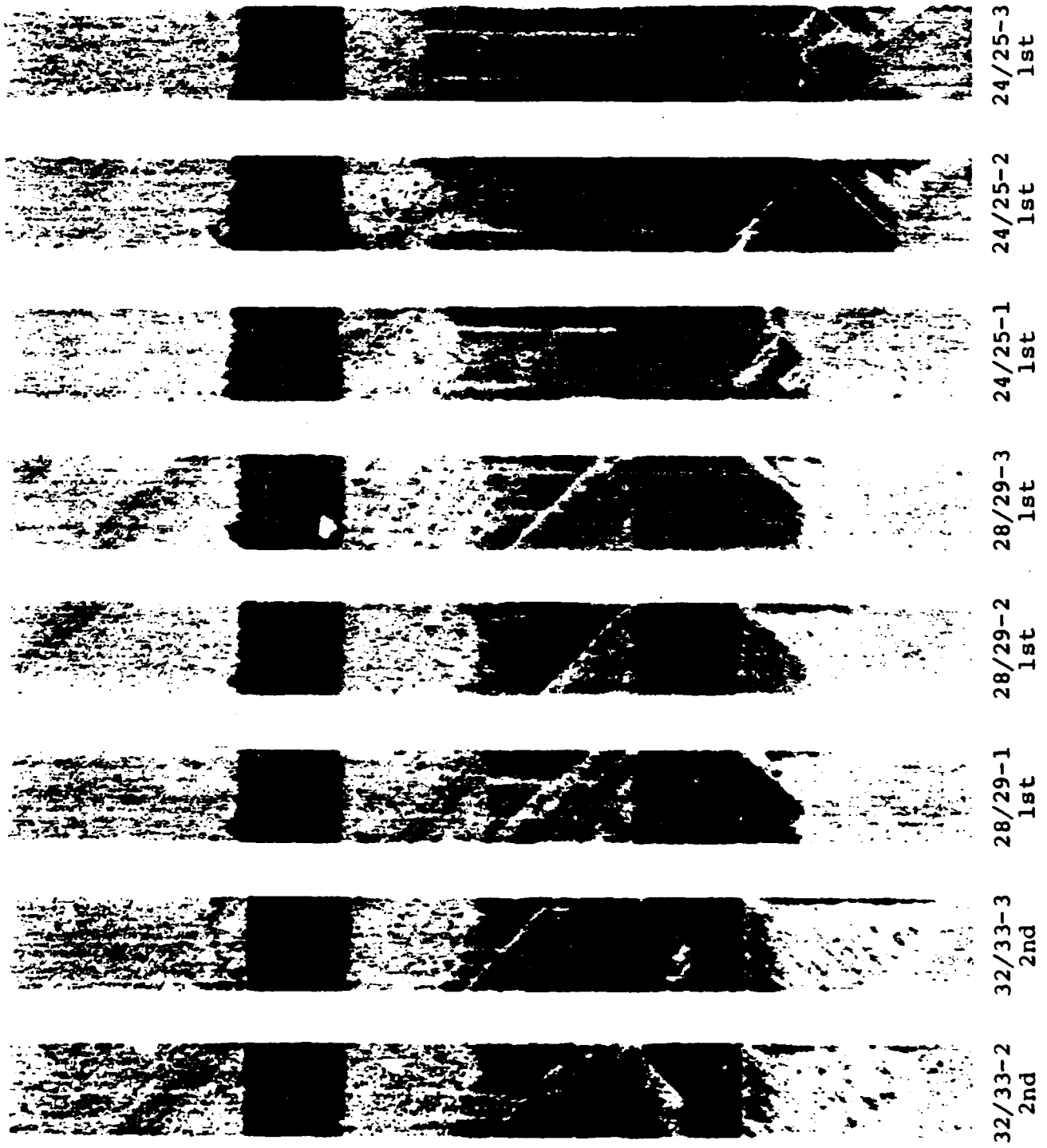
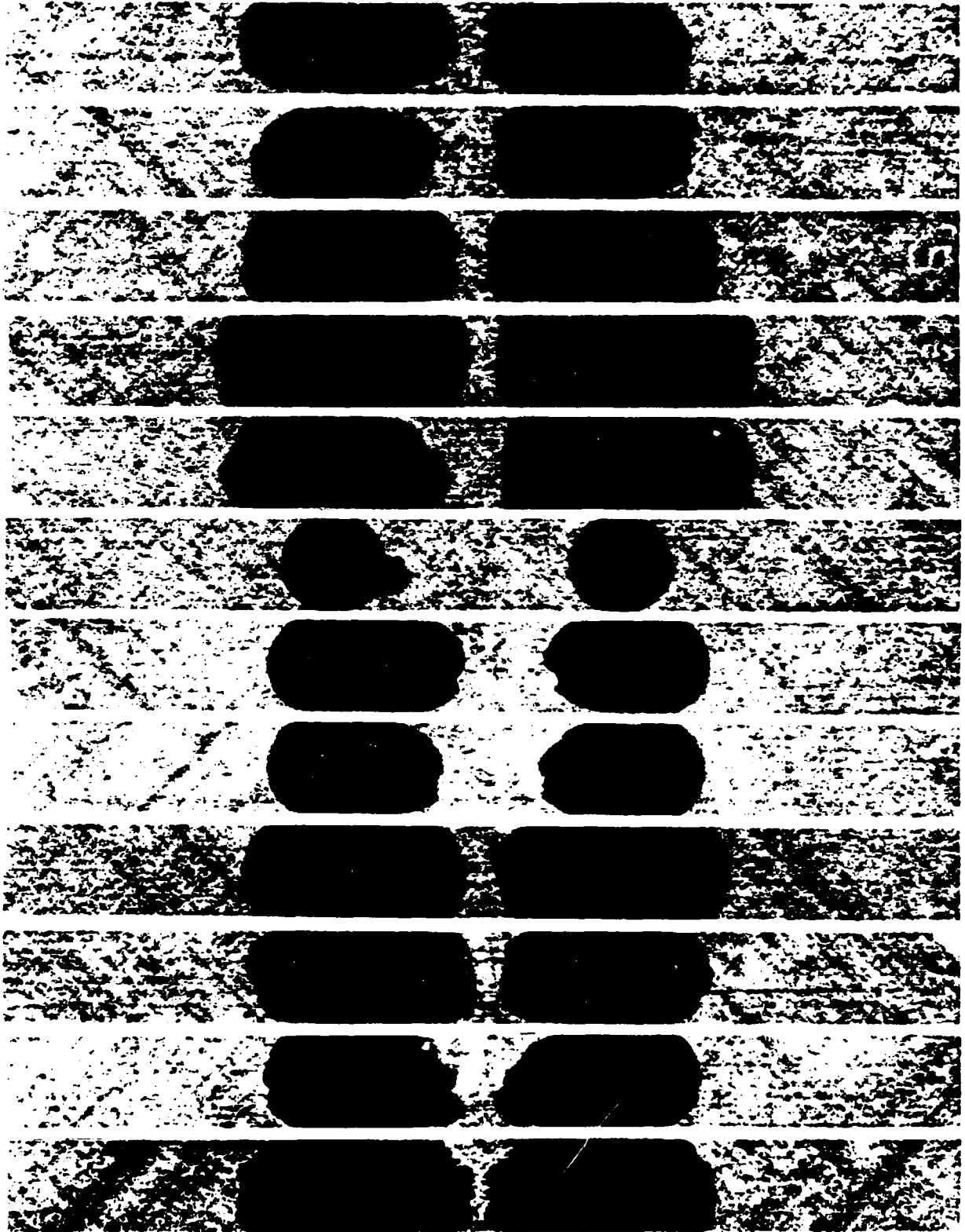


Figure 3. Representative C-scans After Load Drop and Prior to Complete Failure -



S-3 S-4 S-5 S-6 S-10 S-12 S-13 S-14 S-15 S-16 S-17 S-18

Figure 4. C-scans of Sharp Crack Specimens - Task II

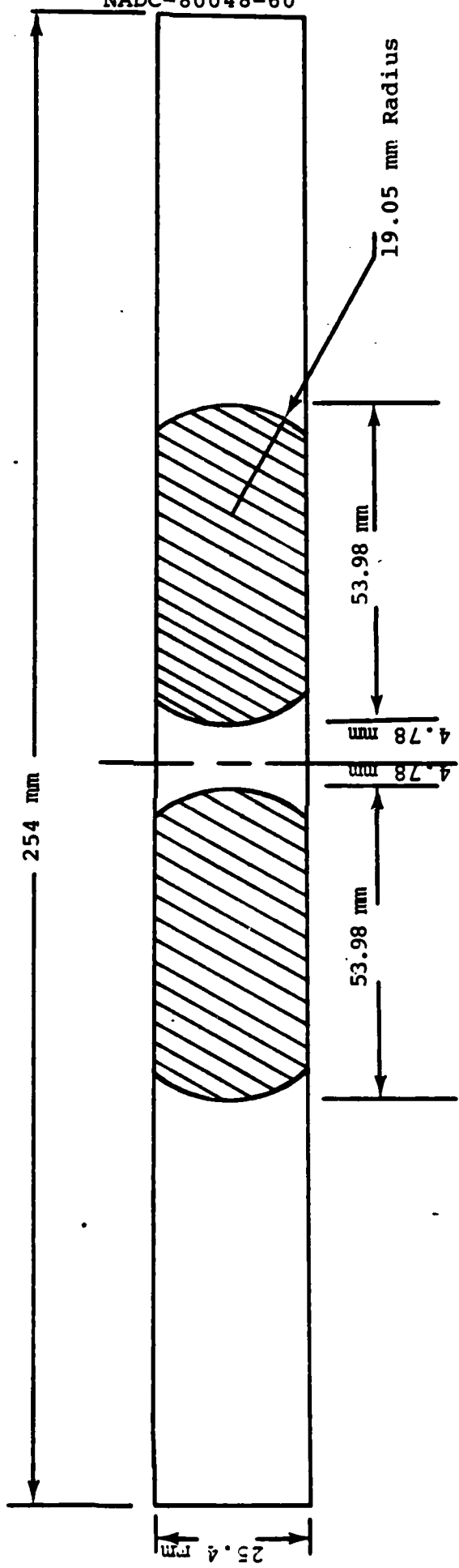
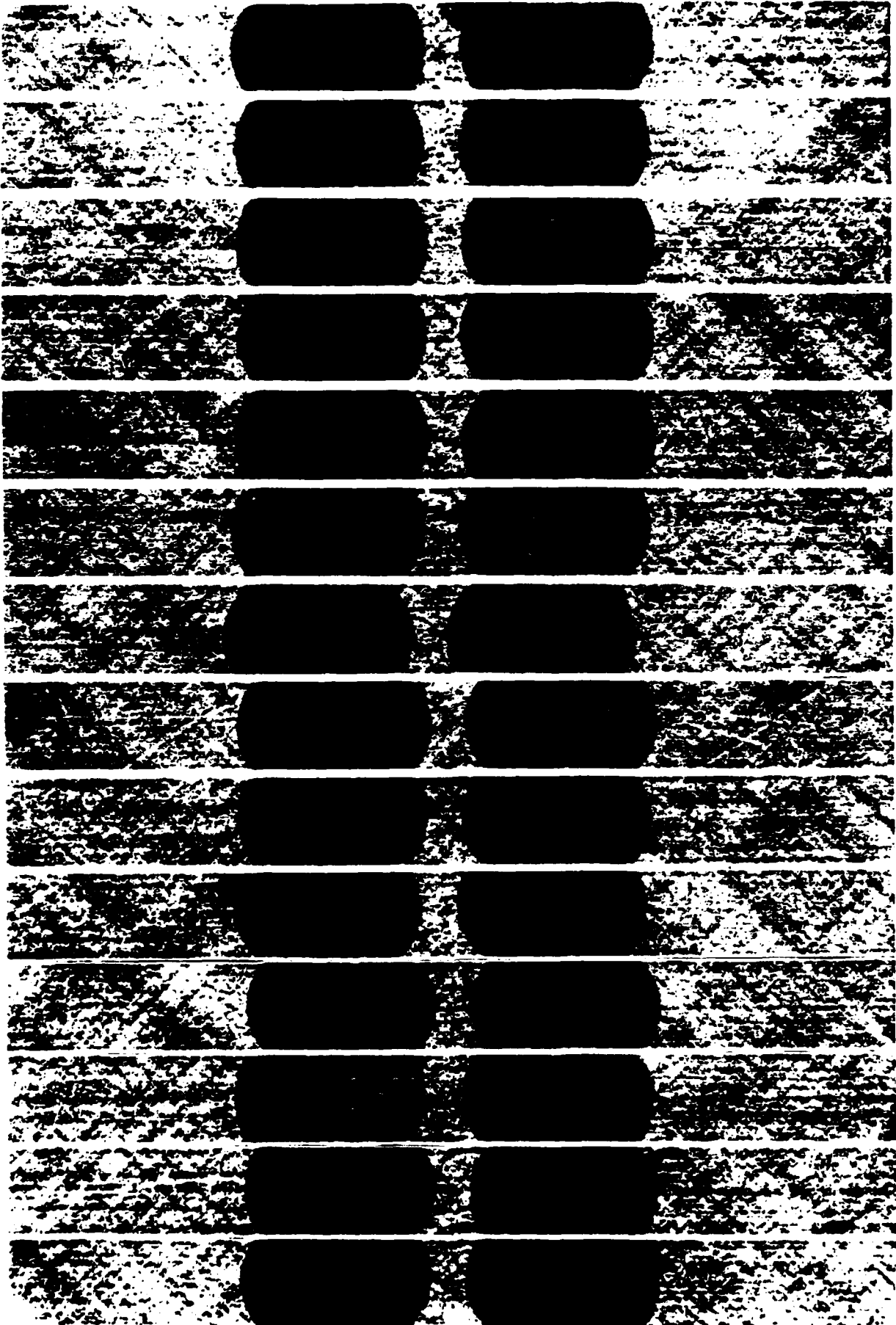


Figure 5. Blunt Crack Sample Geometry



B1 B2 B3 B4 B5 B6 B7 B8 B9 B10 B11 B12 B13 B14

Figure 6. C-scans of Blunt Crack Specimens - Task II

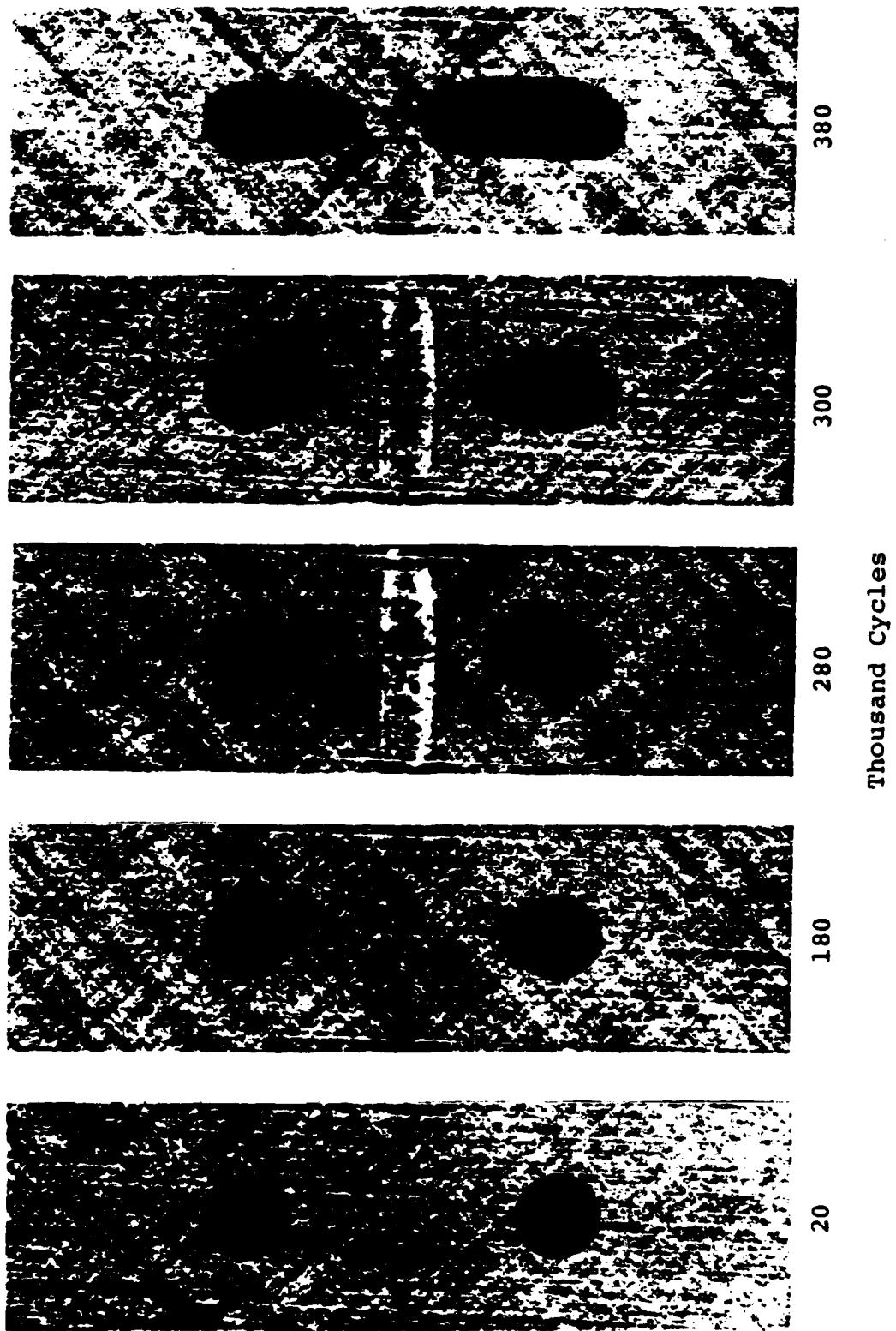


Figure 7. Flaw Growth in Sample 3-1RO-1, S = 0.5

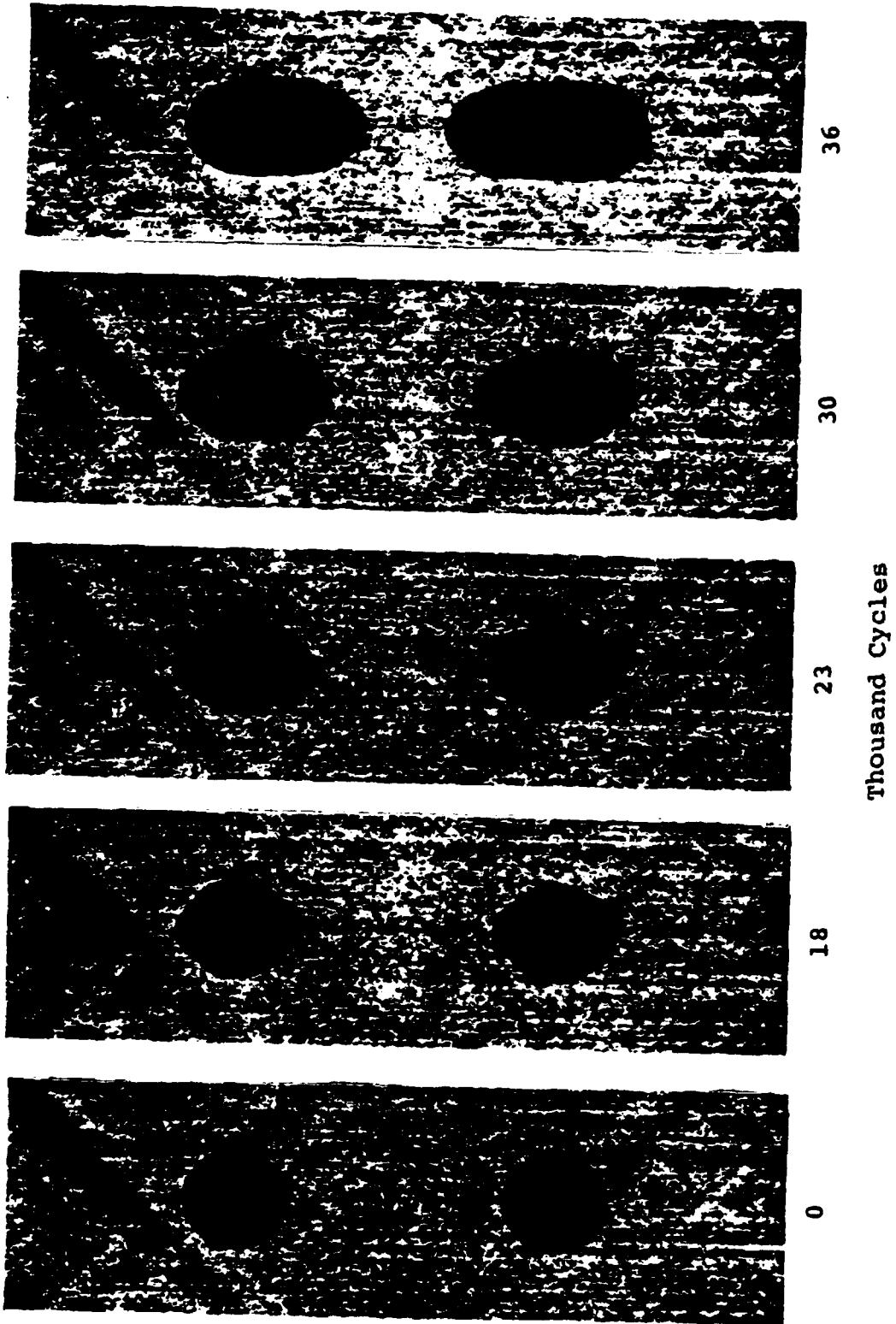


Figure 8. Flaw Growth in Sample 3-125RO-1, $S = 0.5$

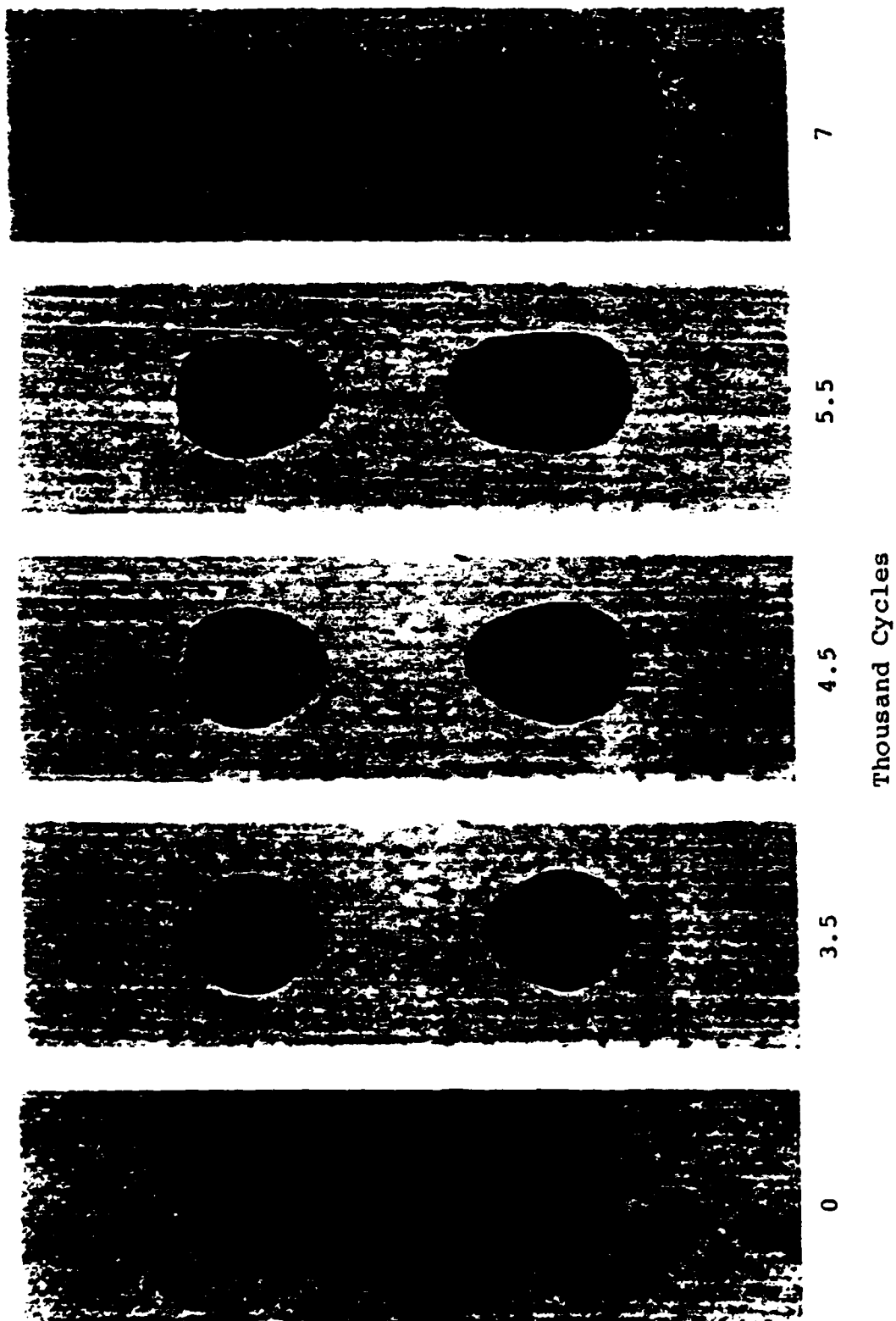


Figure 9. Flaw Growth in Sample 3-150RO-1, S = 0.5

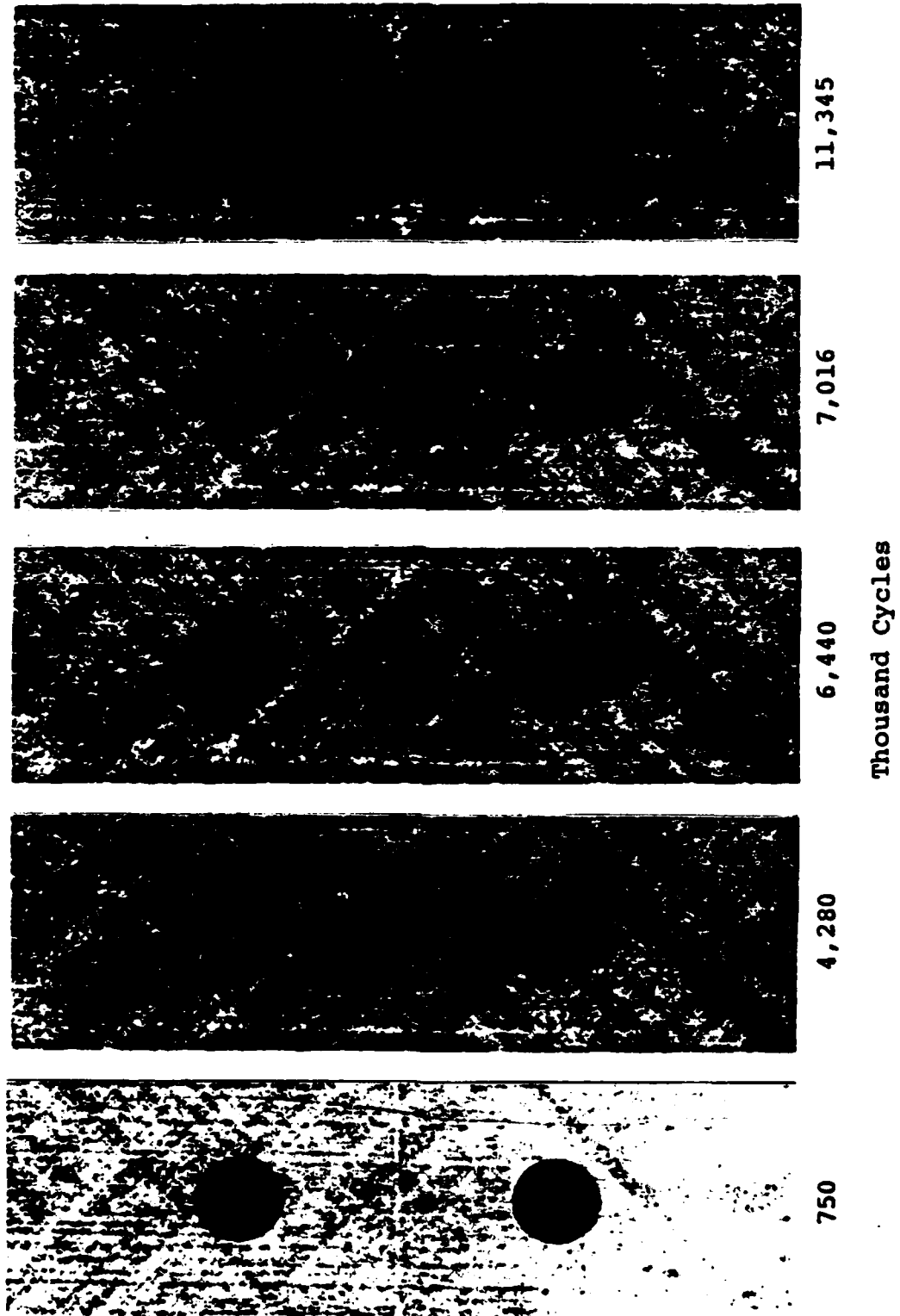


Figure 10. Flaw Growth in Sample 3-1R+25-2, S = 0.5

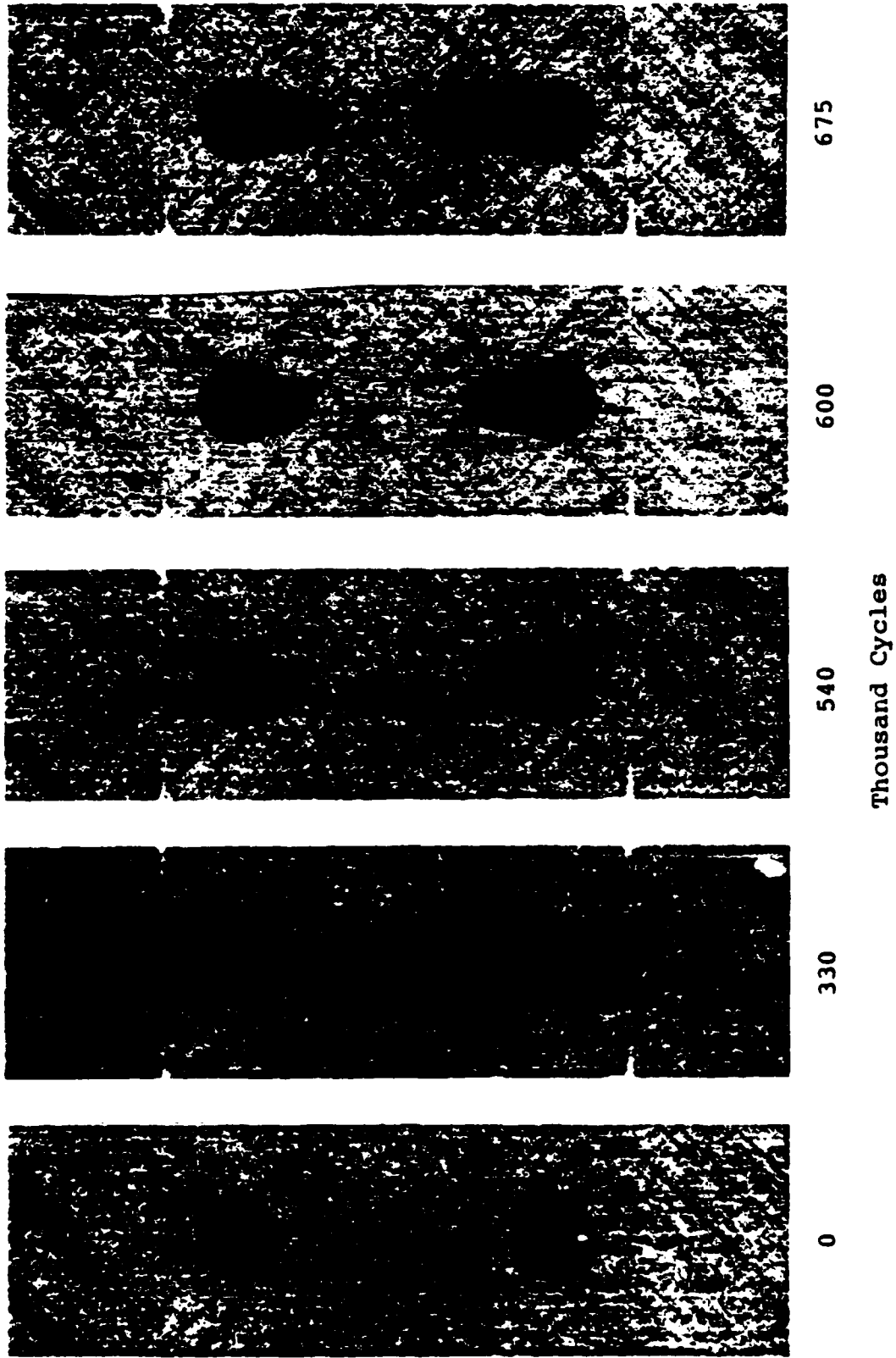


Figure 11. Flaw Growth in Sample 3-1R-25-2, S = 0.5

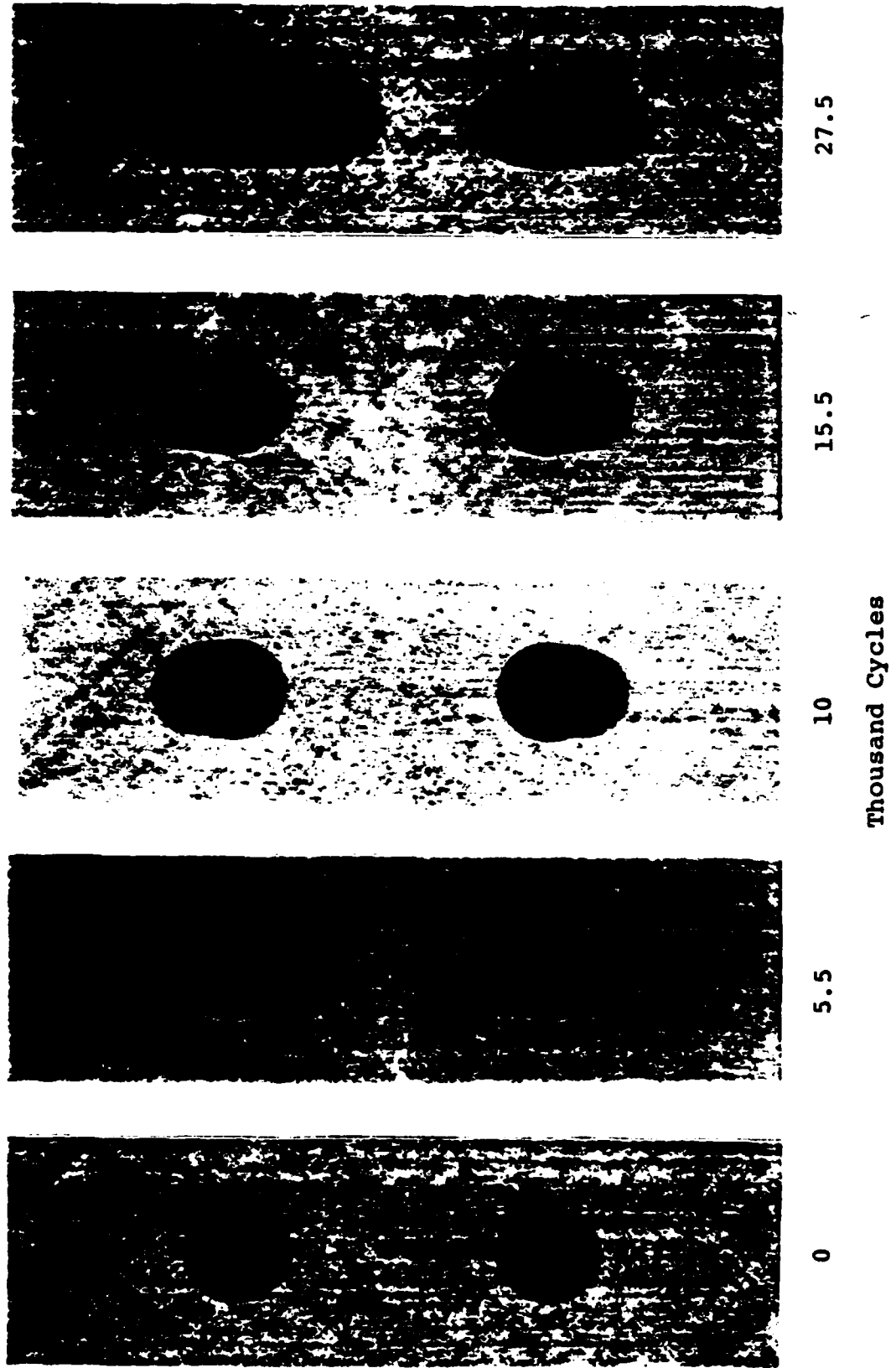


Figure 12. Flaw Growth in Sample 3-125R+25-1, S = 0.75

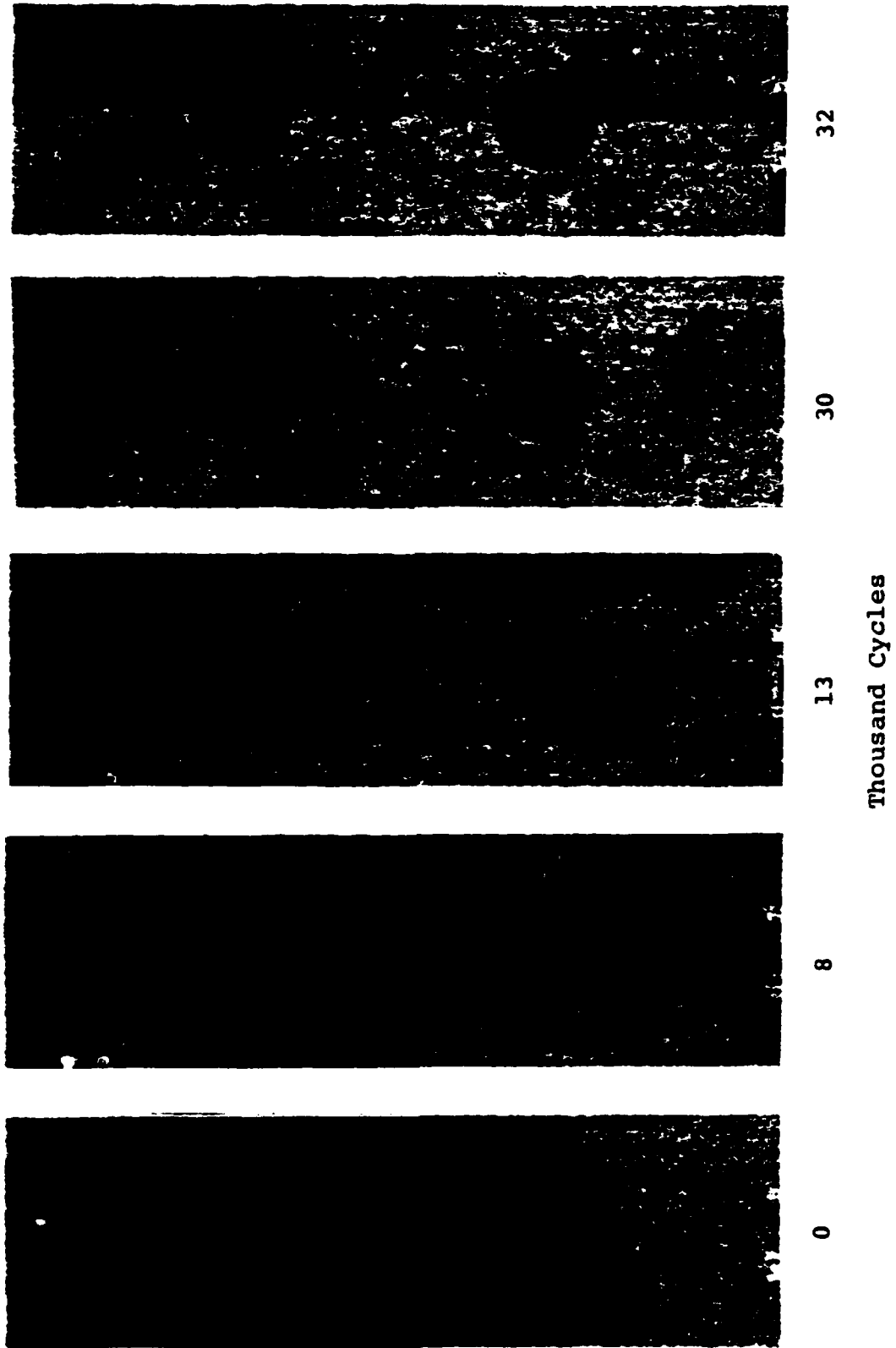


Figure 13. Flaw Growth in Sample 3-125R-25-2, S = 0.5

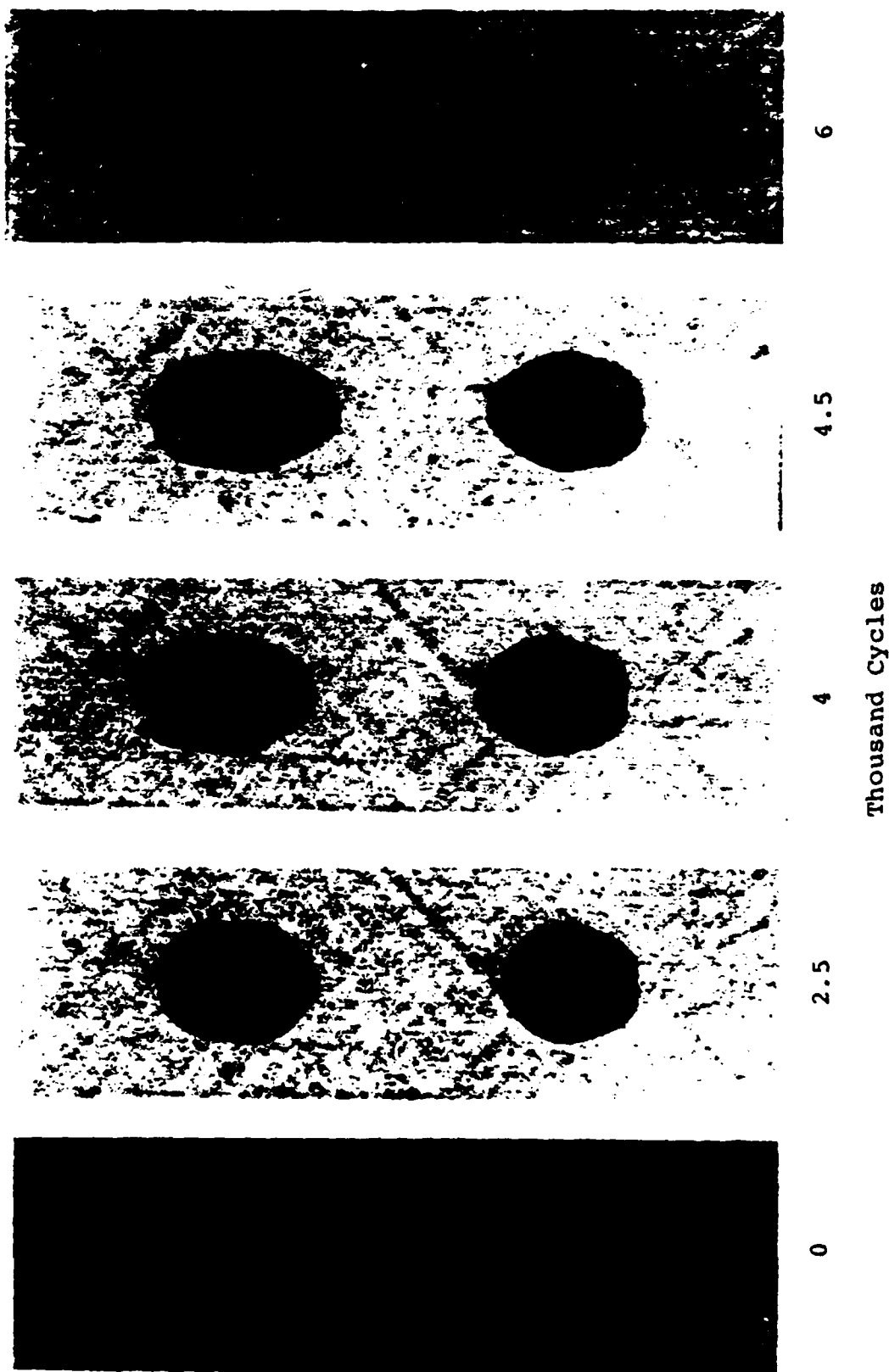


Figure 14. Flaw Growth in Sample 3-150R+25-3, S = 0.75

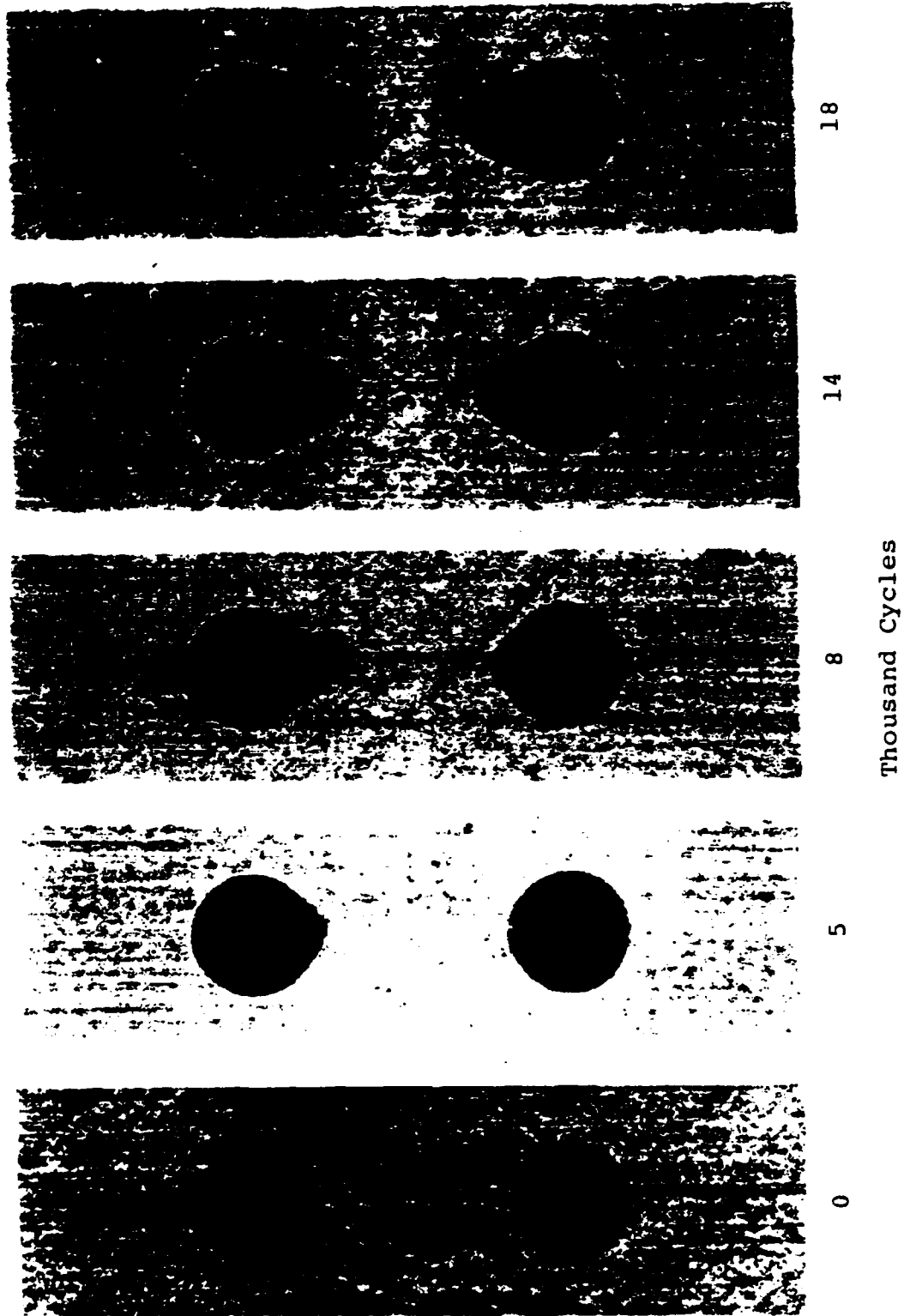


Figure 15. Flaw Growth in Sample 3-150R-25-1, S = 0.5

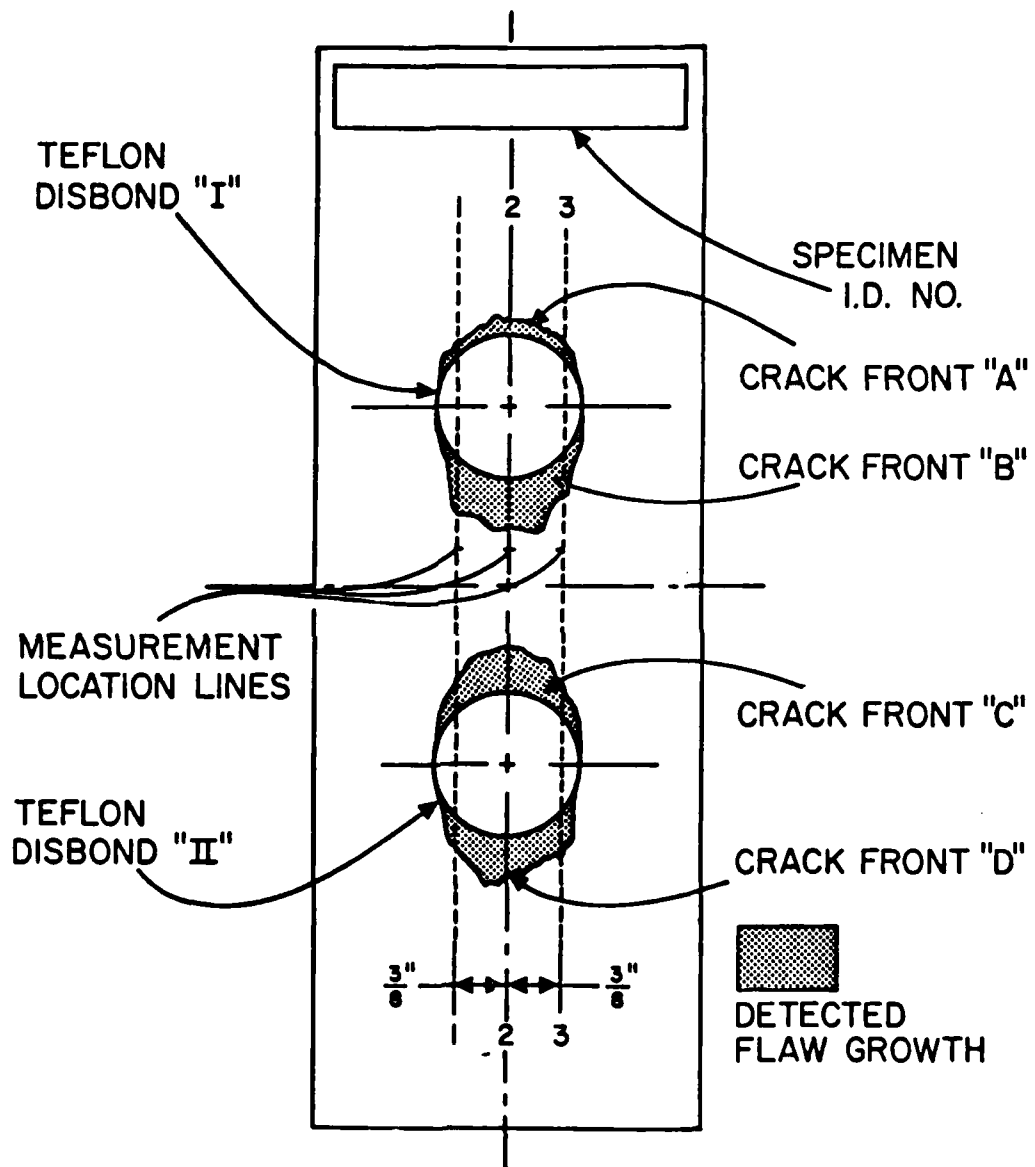


Figure 16. Measurement Locations for Four Crack Fronts

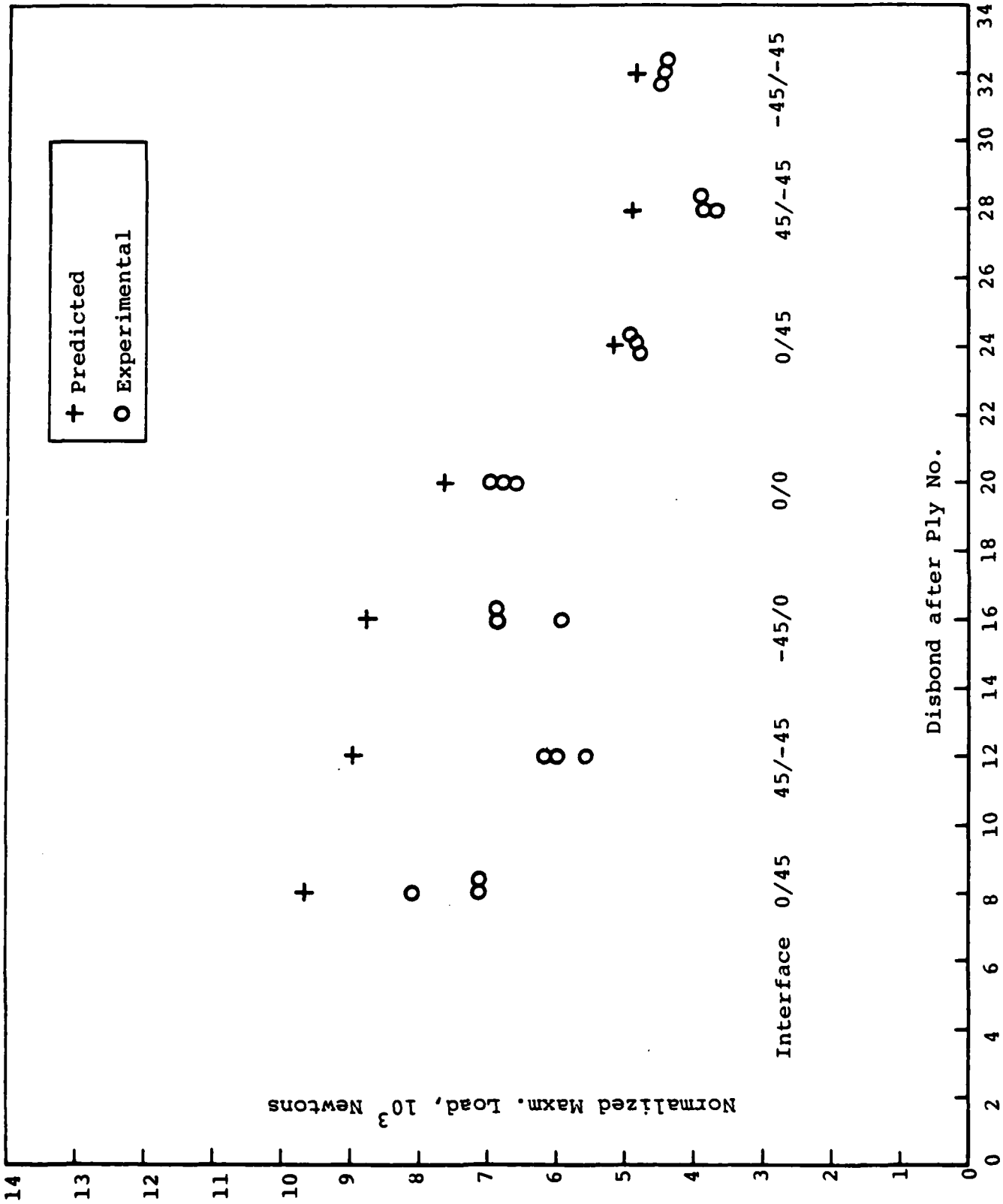


Figure 17. Failure Loads for Disbonds of 2.54 cm. Length in 2.54 cm. Wide Beams-Type A Laminates

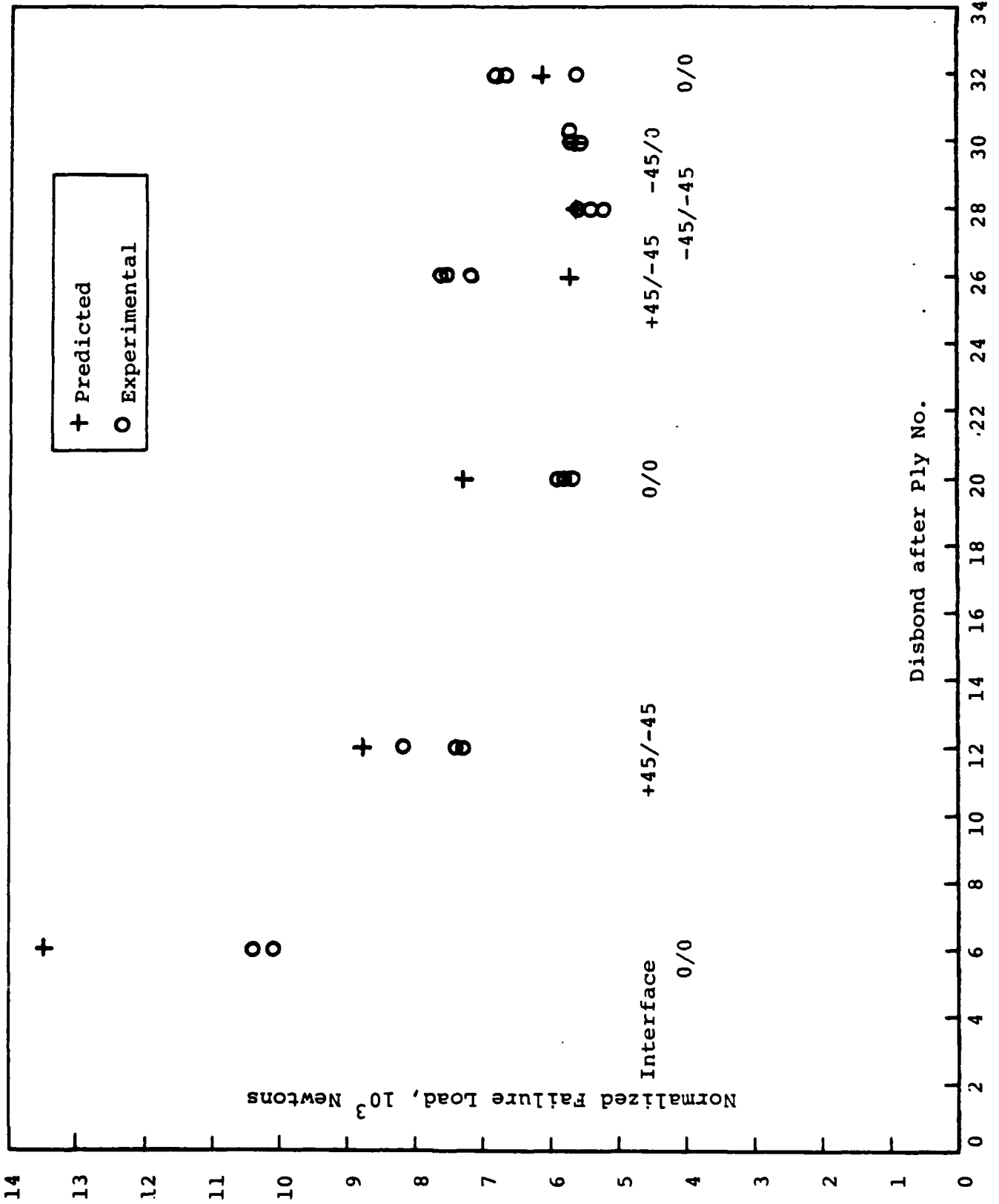


Figure 18. Failure Loads for Disbonds of 2.54 cm. Length in 2.54 cm. Wide Beams-Type B Laminates

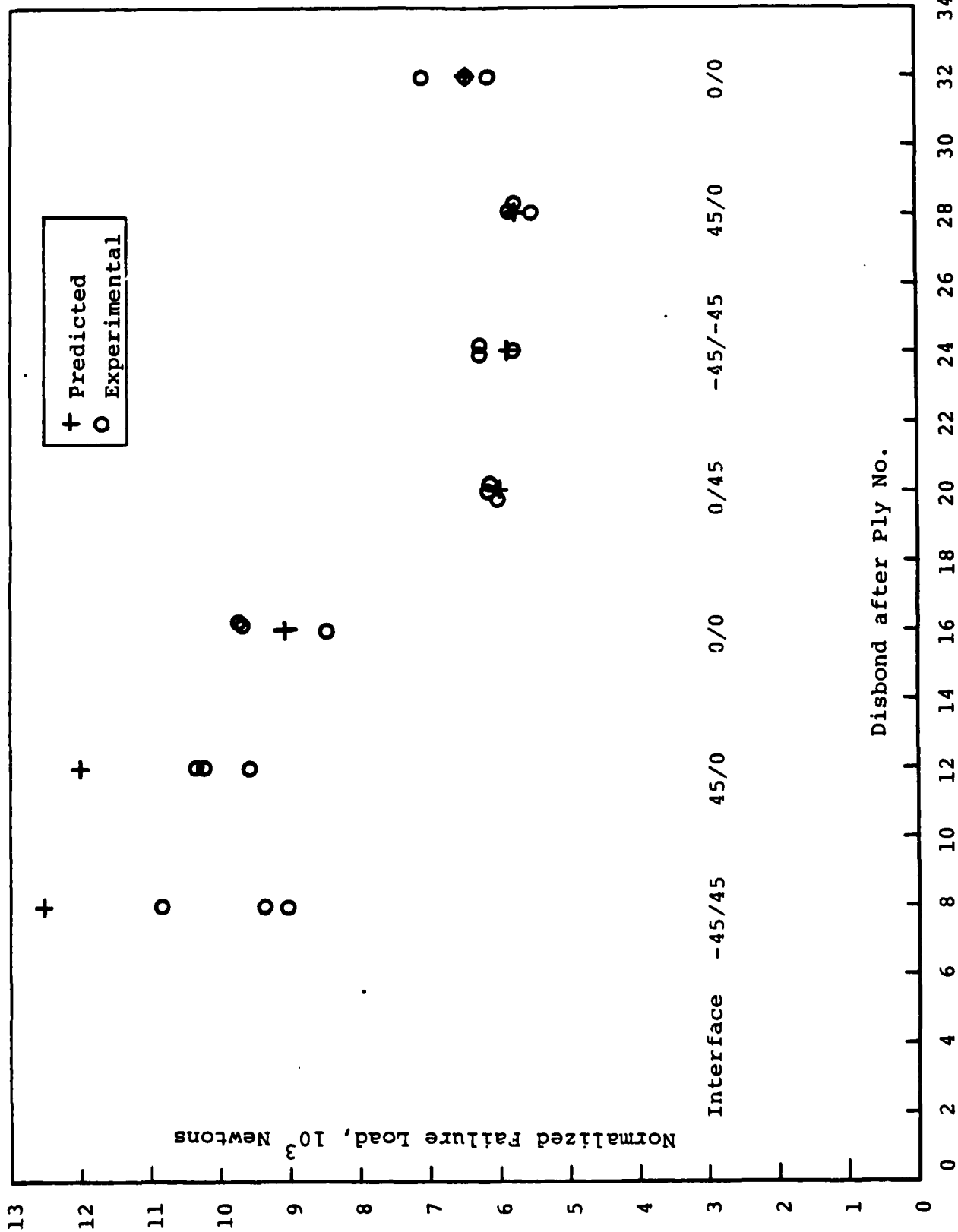


Figure 19. Failure Loads for Disbonds of 2.54 cm. Length in 2.54 cm, Wide Beams-Type C Laminates

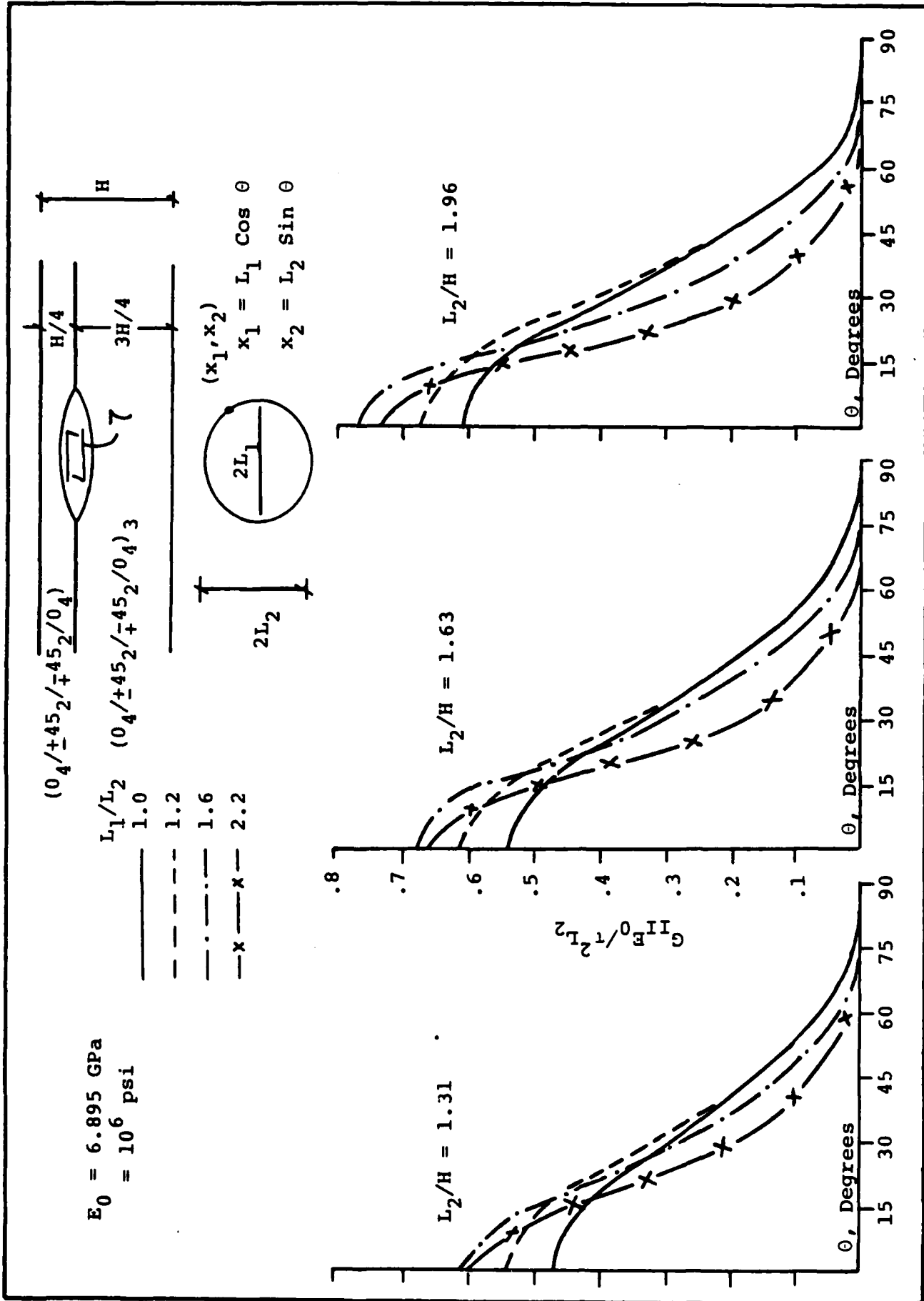


Figure 20. Variation of G_{II} with Dimensions for Flaws at $Z = \pm 0.25H$

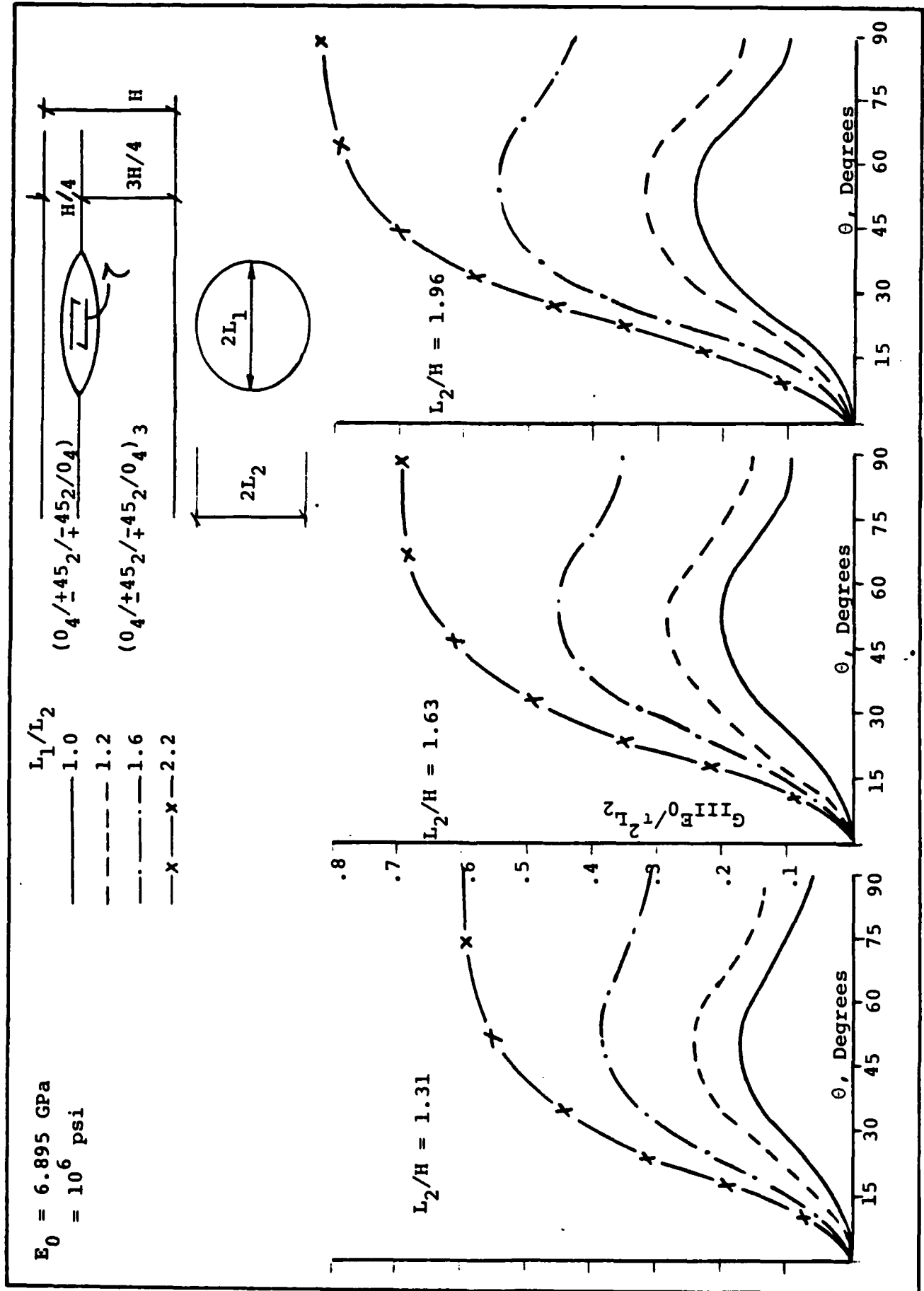


Figure 21. Variation of G_{III} with Dimensions for Flaws at $z = \pm 0.25H$

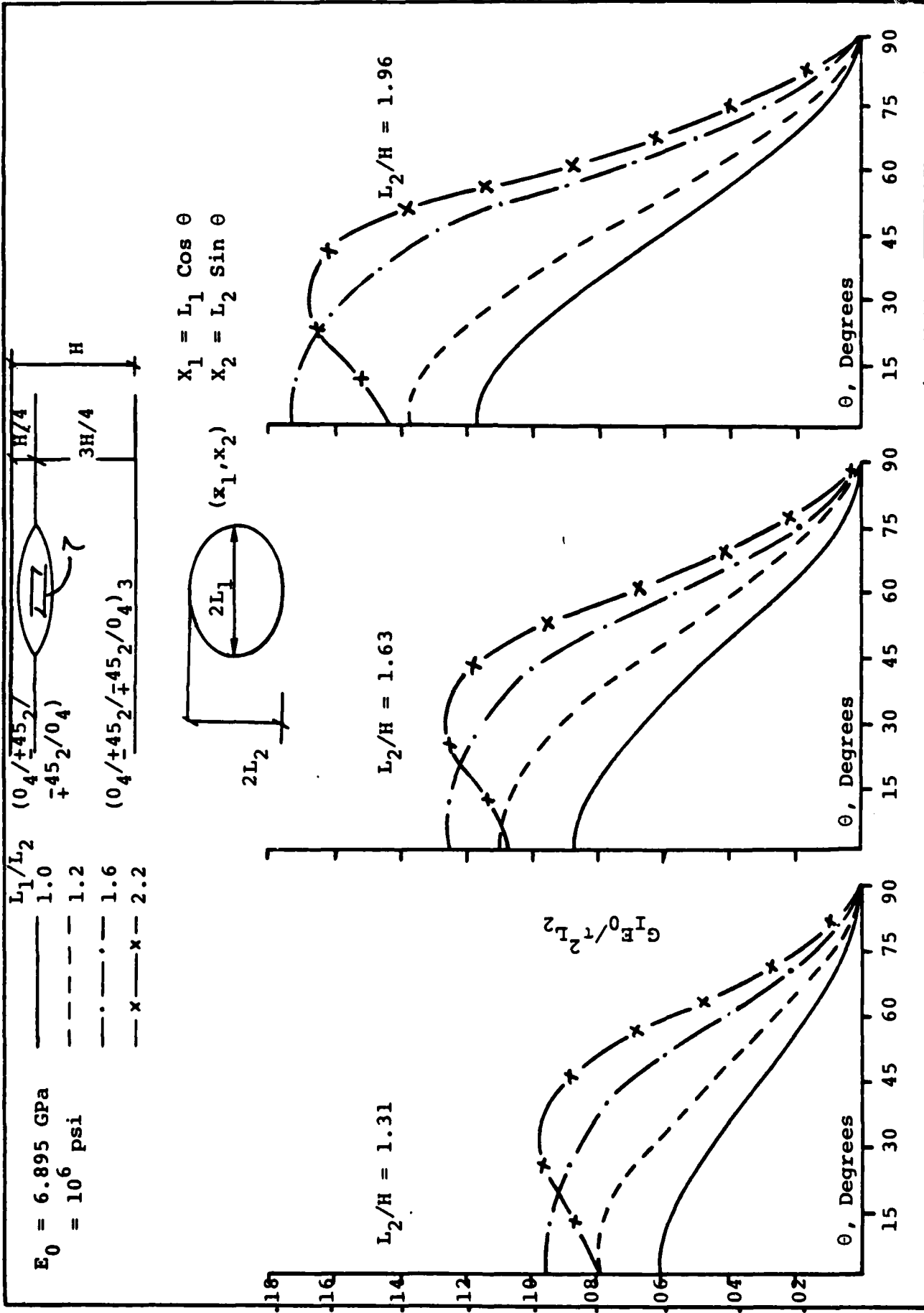


Figure 22. Variation of G_I with Dimensions of Flaw at $z = \pm 0.25H$

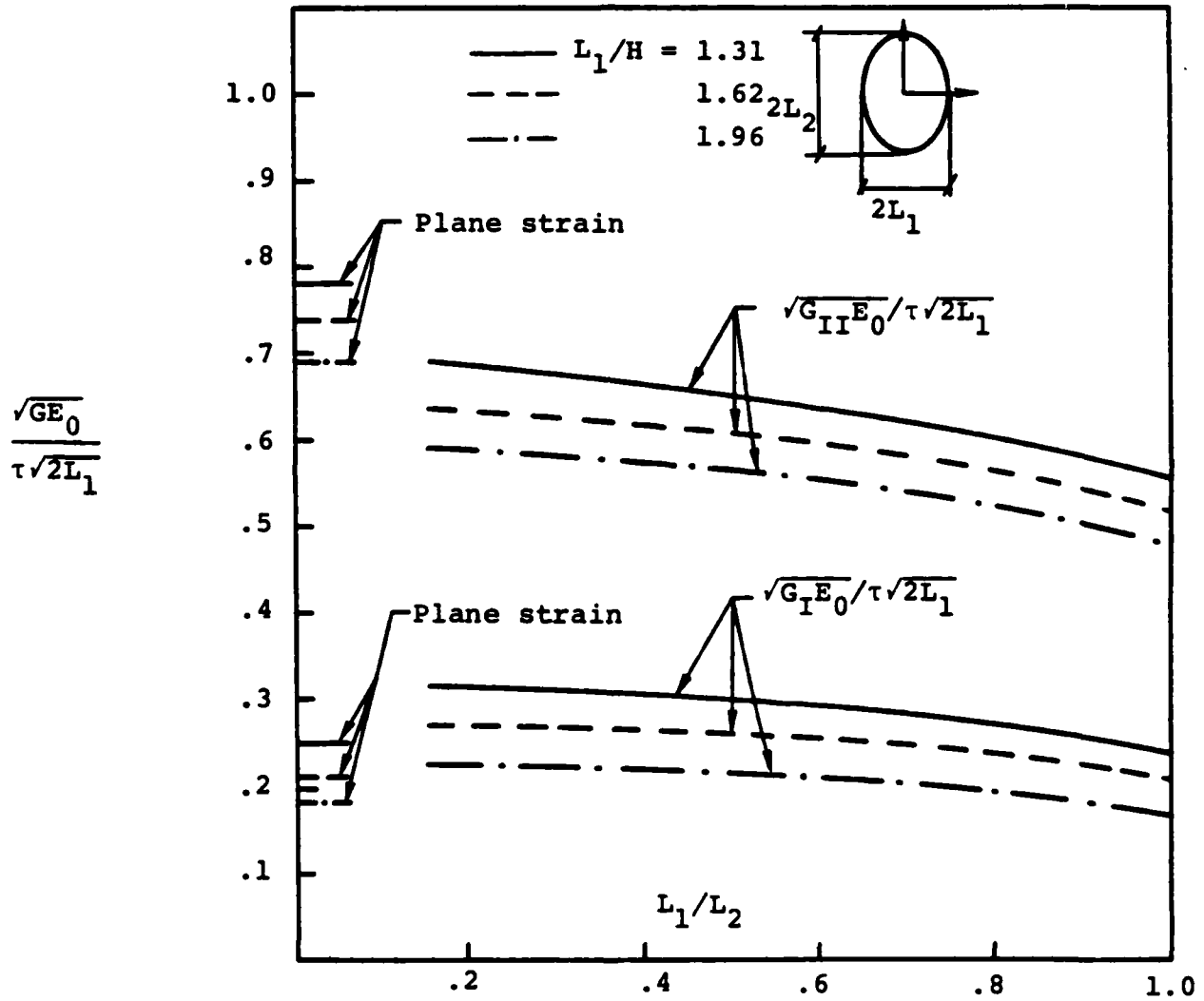


Figure 23. Variation of G_I and G_{II} with L_1/L_2

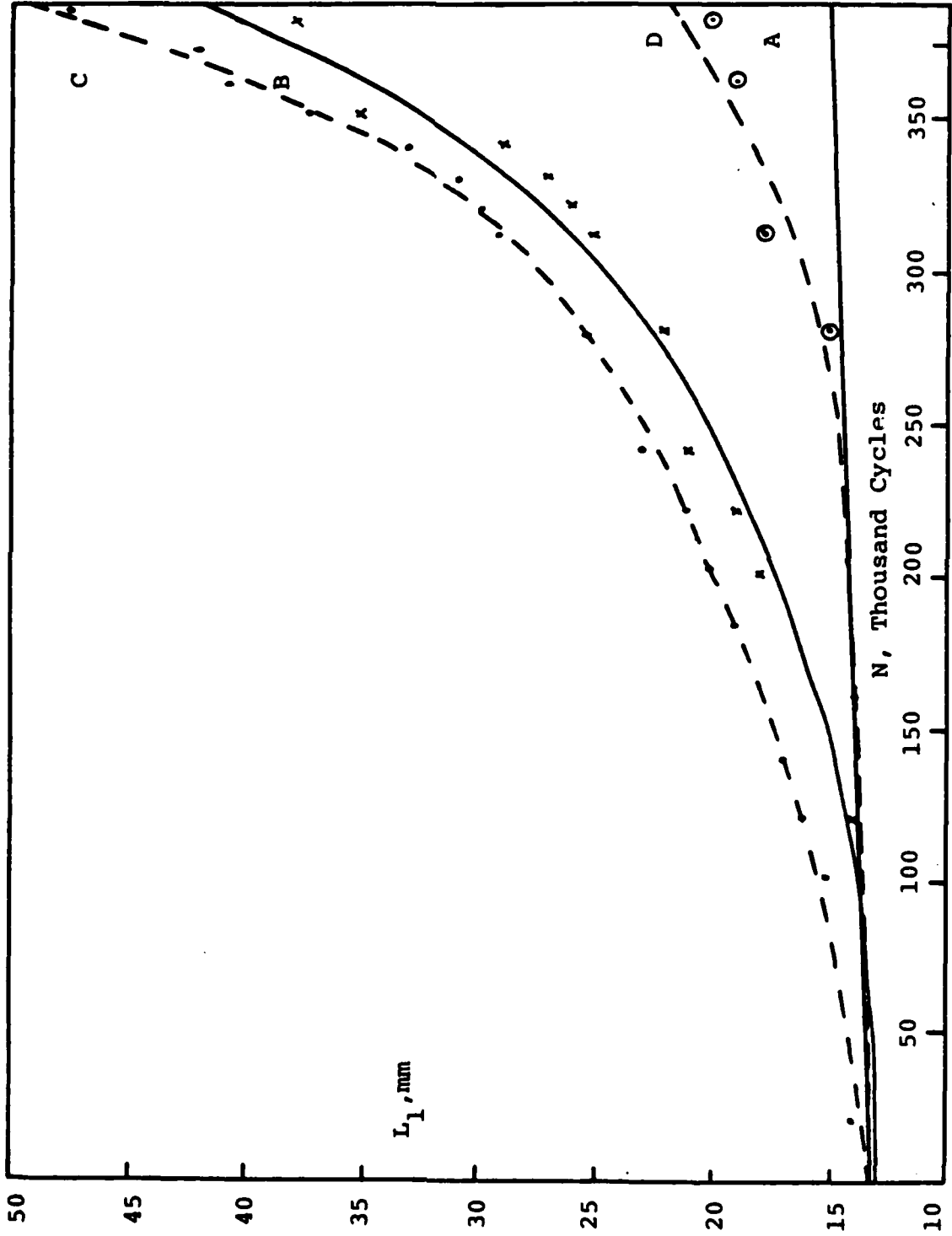


Figure 24. L_1 vs. N , Sample 3-1RO-1, $S = 0.5$

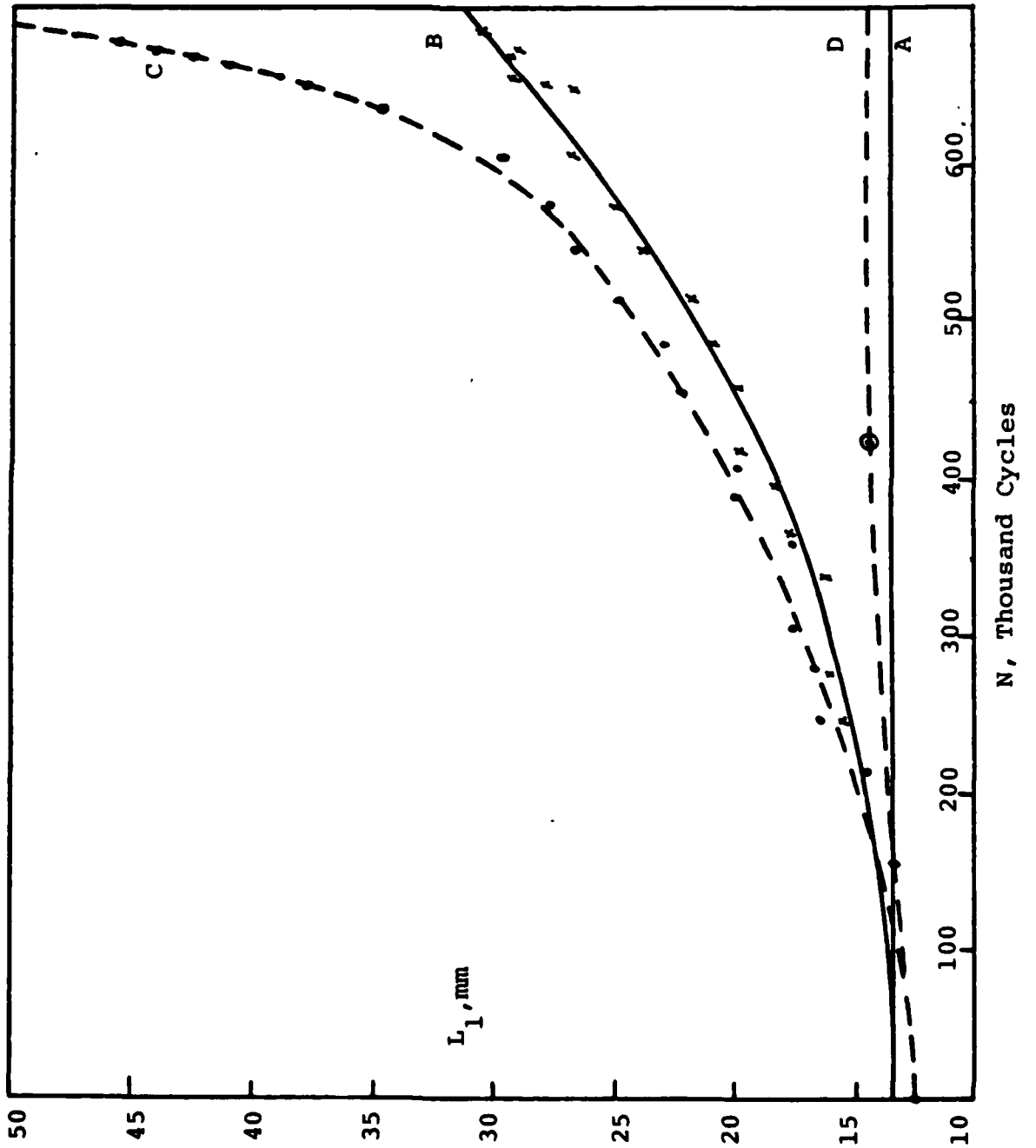


Figure 25. L_1 vs. N , Sample 3-1R-25-2, $s = 0.5$

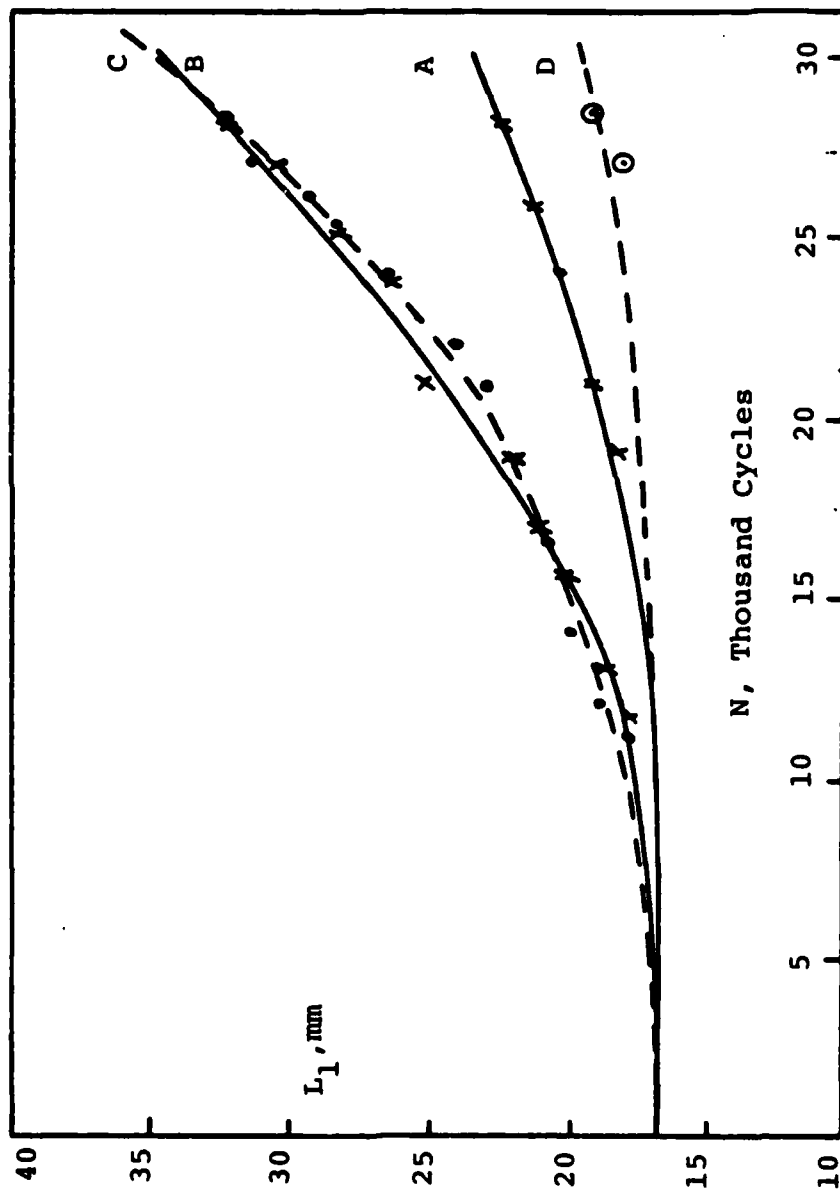


Figure 26. L_1 vs. N , Sample 3-125R0-2, $S = 0.5$

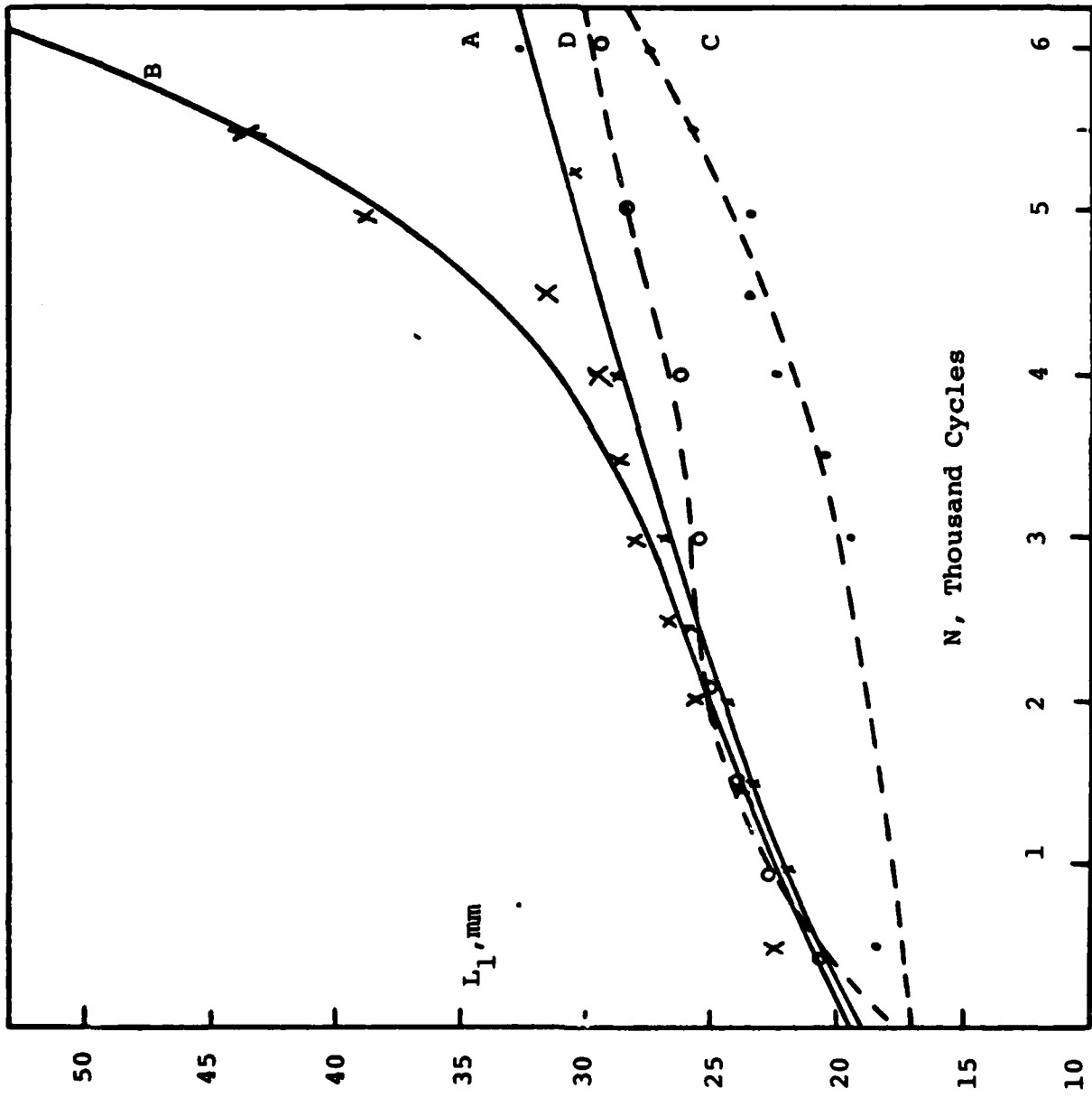


Figure 27. L_1 vs. N , Sample 3-150R+25-3, $S = 0.75$

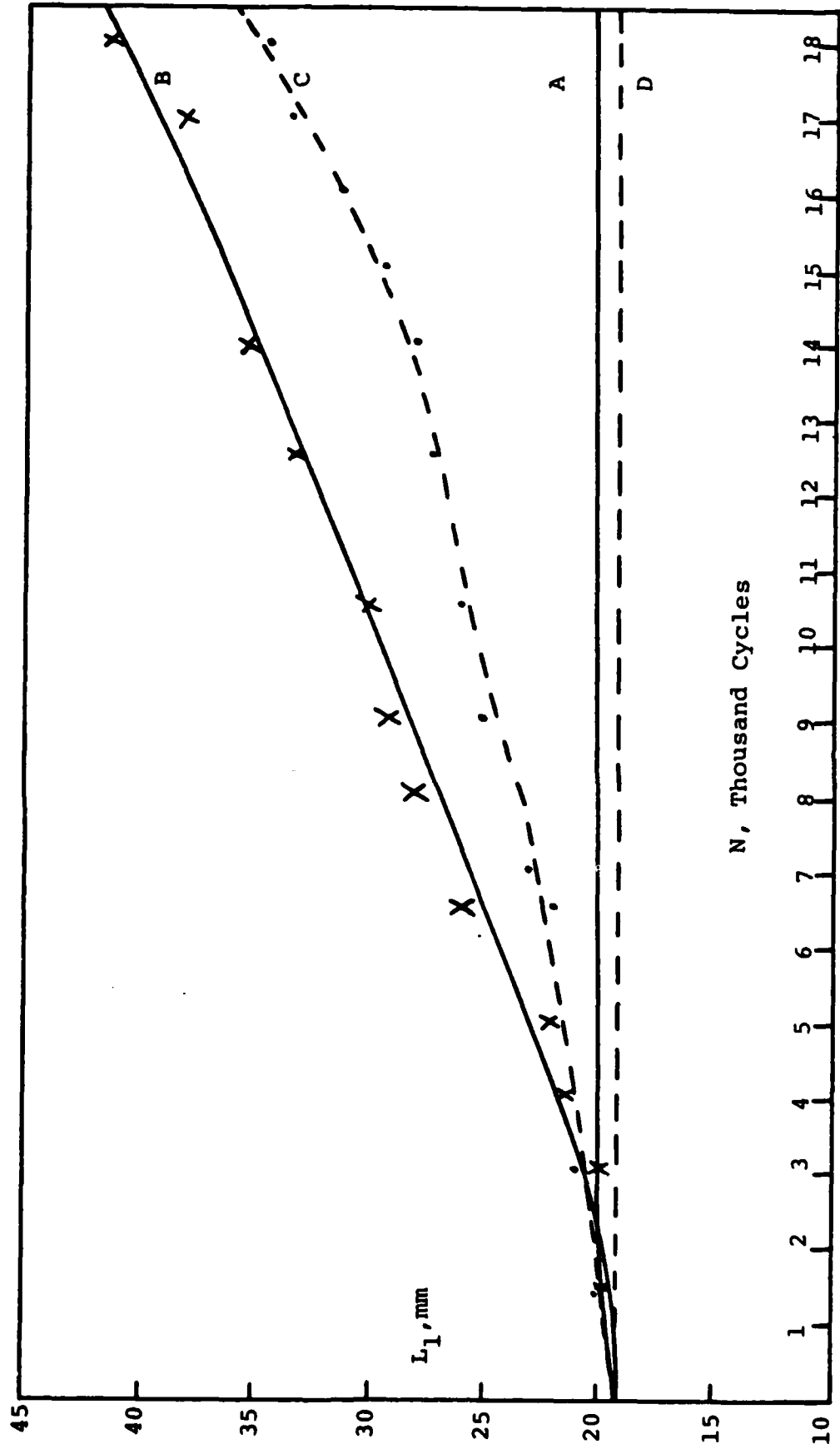


Figure 28. L_1 vs. N , Sample 3-150R-25-1, $s = 0.5$

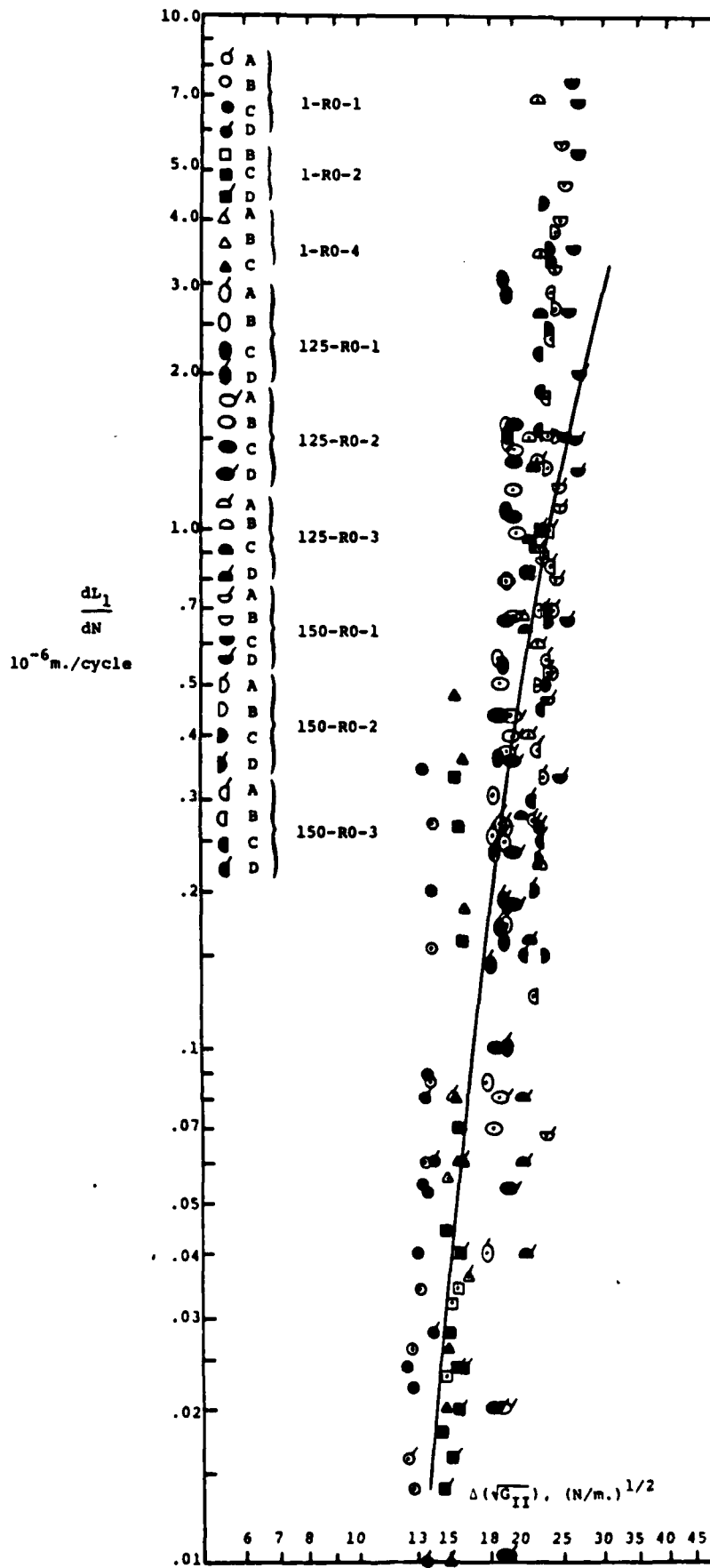


Figure 29. Growth of Disbands in Midplane, $Z=0$, $S=0.5$

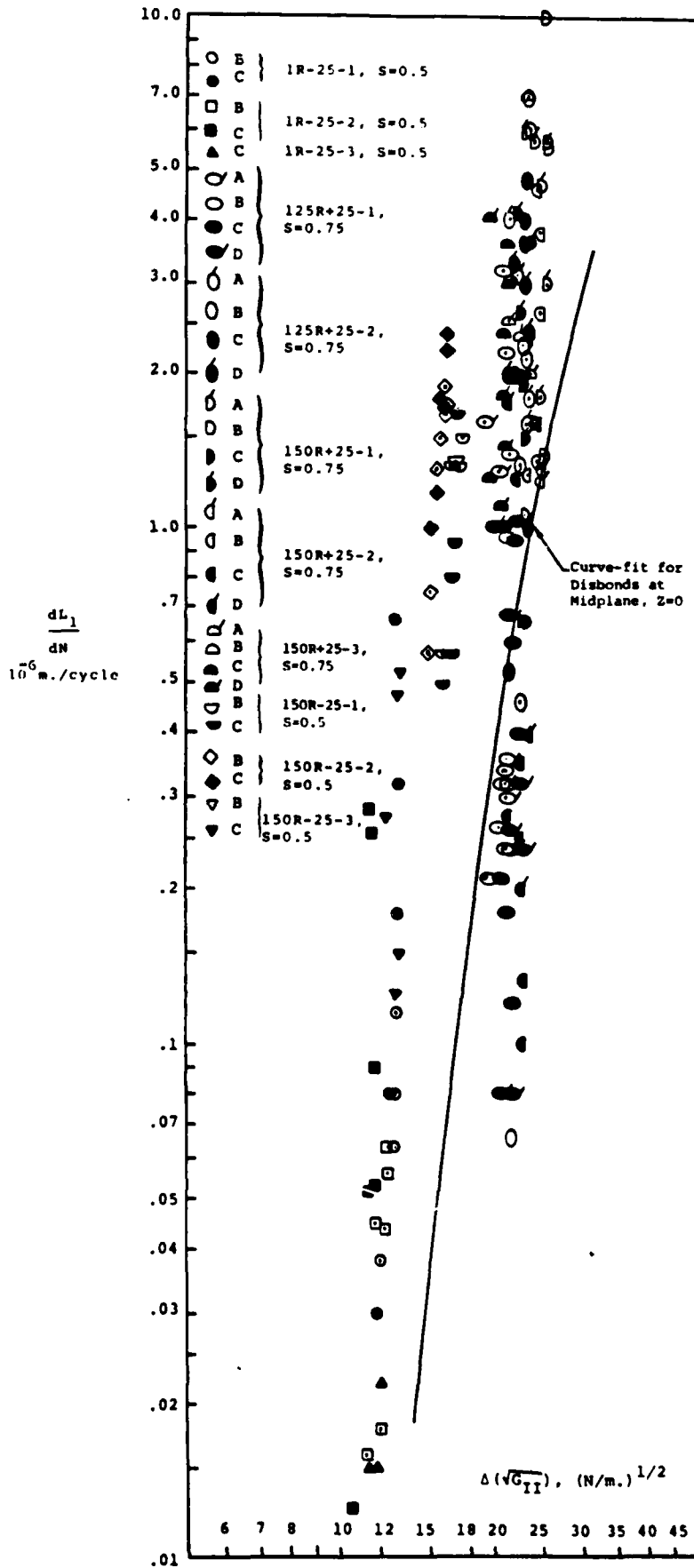


Figure 30. Growth of Disbands of $\lambda=+0.25H$